

Design Principles and Theory of Paramagnetic Fluorine-Labelled Lanthanide Complexes as Probes for ^{19}F Magnetic Resonance: A Proof-of-Concept Study

Kirsten H. Chalmers,^[a] Elena De Luca,^[a] Naomi H. M. Hogg,^[a] Alan M. Kenwright,^[a]
Ilya Kuprov,^{*,[b]} David Parker,^{*,[a]} Mauro Botta,^[c] J. Ian Wilson,^[d] and
Andrew M. Blamire^[d]

Abstract: The synthesis and spectroscopic properties of a series of CF_3 -labelled lanthanide(III) complexes ($\text{Ln} = \text{Gd}, \text{Tb}, \text{Dy}, \text{Ho}, \text{Er}, \text{Tm}$) with amide-substituted ligands based on 1,4,7,10-tetraazacyclododecane are described. The theoretical contributions of the ^{19}F magnetic relaxation processes in these systems are critically assessed and selected volumetric plots are presented. These plots allow an accurate estimation of the increase in the rates of longitudinal and transverse relaxation as a function of the distance between the Ln^{III} ion and the fluorine nucleus, the applied magnetic field, and the re-rotational correlation time of the complex,

for a given Ln^{III} ion. Selected complexes exhibit pH-dependent chemical shift behaviour, and a $\text{p}K_{\text{a}}$ of 7.0 was determined in one example based on the holmium complex of an *ortho*-cyano DO3A-monoamide ligand, which allowed the pH to be assessed by measuring the difference in chemical shift (varying by over 14 ppm) between two ^{19}F resonances. Relaxation analyses of variable-temperature and variable-field ^{19}F , ^{17}O and ^1H NMR

spectroscopy experiments are reported, aided by identification of salient low-energy conformers by using density functional theory. The study of fluorine relaxation rates, over a field range of 4.7 to 16.5 T allowed precise computation of the distance between the Ln^{III} ion and the CF_3 reporter group by using global fitting methods. The sensitivity benefits of using such paramagnetic fluorinated probes in ^{19}F NMR spectroscopic studies are quantified in preliminary spectroscopic and imaging experiments with respect to a diamagnetic yttrium(III) analogue.

Keywords: fluorine • imaging agents • lanthanides • magnetic properties • NMR spectroscopy

Introduction

Over the past twenty years, magnetic resonance imaging (MRI) has become one of the most important diagnostic tools in clinical practice. MRI instrumentation operating at 1.4 to 9.4 T is widely available and has been used with great success for solving problems as diverse as cancer diagnostics,^[1] catalyst design^[2] and the identification of Egyptian mummies.^[3] The advent of MRI contrast agents based on super-paramagnetic iron oxide particles^[4] and Gd^{III} complexes^[5] has enhanced the quality of information that can be obtained from medical MRI scans by allowing certain tissues or regions of the body to be selectively highlighted. Contrast remains a difficult issue though; standard instruments use ^1H nuclei, and the concentration and relaxation rate of protons in certain tissues is frequently similar.^[6]

It has long been recognised that standard MRI instruments can be easily re-tuned from ^1H to ^{19}F nuclei, which have very similar magnetic properties.^[7] This has stimulated the development of binuclear $^1\text{H}/^{19}\text{F}$ imaging probes and re-

[a] K. H. Chalmers, E. D. Luca, N. H. M. Hogg, Dr. A. M. Kenwright, Prof. D. Parker
Department of Chemistry
Durham University
South Road, Durham, DH1 3LE (UK)
E-mail: david.parker@dur.ac.uk

[b] Dr. I. Kuprov
Oxford e-Research Centre
7 Keble Road, Oxford, OX1 3QG (UK)
E-mail: ilya.kuprov@oerc.ox.ac.uk

[c] Prof. M. Botta
Dipartimento di Scienze dell' Ambiente e della Vita
Università del Piemonte Orientale, "Amedeo Avogadro"
Viale Teresa Michel 11, 15100, Alessandria (Italy)

[d] Dr. J. I. Wilson, Prof. A. M. Blamire
Newcastle Magnetic Resonance Centre
Newcastle University, Campus for Ageing and Vitality
Newcastle-upon-Tyne, NE4 5PL (UK)

Supporting information for this article is available on the WWW under <http://dx.doi.org/10.1002/chem.200902300>.

search into fluorinated materials suitable for detection in vivo.^[8,9] The published works range from quantitative NMR spectroscopic tracking of the metabolism of fluorinated drugs^[10] to imaging studies of organ inflammation processes by using chemically inert perfluorinated compounds as contrast agents.^[11] Perfluorocarbons have also been used to signal changes in local oxygen pressure as a consequence of their interaction with this paramagnetic species in vivo.^[9b]

Several reports have addressed functional ¹⁹F MRI probes in which the observed signal reports a change in the chemical state of the probe. These include systems designed to detect an irreversible chemical transformation of the fluorinated probe, for example, a cleavage reaction catalysed by an enzyme.^[12] The limiting features of this approach include the irreversibility of the chemical transformation and the modest change in the observed ¹⁹F shift, typically $\delta \leq 2$ ppm for pH-independent systems.^[9b,13] A more promising approach involves a probe that undergoes a continuous and reversible transformation as a function of a given parameter so that the observed changes in chemical shift can be calibrated to report, for example, the local pH.^[7] Using the chemical shift (rather than signal intensity) as a reporter also avoids the problems associated with variations in probe concentration.^[12b-e]

As in most magnetic resonance techniques, sensitivity is a key issue with ¹⁹F NMR spectroscopy and MRI. The obvious strategy for improving the sensitivity is to increase the local concentration of the probe. Alternatively, the longitudinal ¹⁹F relaxation can be accelerated by introducing a proximate paramagnetic centre (e.g., Ln³⁺ or Mn²⁺).^[13,14] Relaxation enhancements of at least two orders of magnitude are frequently achieved, which may give rise to an order of magnitude increase in signal intensity. In practice, a balance needs to be struck between the benefits of relaxation enhancement and the reduced detection sensitivity associated with broader spectral lines, given that transverse relaxation is also enhanced.^[13b]

The standard method of generating paramagnetic relaxation enhancement (originally developed to assist ¹³C and ¹⁵N NMR spectroscopy^[15]) involves adding a paramagnetic agent to the sample. At low probe concentrations, however, the improvement is quite modest^[16] because the encounter probability between the fluorinated reporter group and the paramagnetic molecule is quite low. Better results are achieved if the contact time is increased by, for example, ion-pairing^[17] or reversible coordination.^[18]

An alternative approach that we introduced,^[13,14] involves carefully positioning a CF₃ reporter group within 7 Å of a paramagnetic centre (a lanthanide(III) ion) located in the same complex. With different lanthanide ions, the resulting complex can function either as a fluorine magnetic resonance probe (with moderate relaxation enhancers, such as Tb³⁺, Dy³⁺, Ho³⁺, Er³⁺ or Tm³⁺)^[19] or as a ¹H MRI contrast agent with Gd³⁺ for complexes that possess a fast-exchanging water molecule. This dual nature allows two distinct types of experiment: 1) Dual-imaging studies, in which ¹⁹F images are merged with morphologically matched ¹H images to allow the precise anatomic localisation of the ¹⁹F signal intensity^[8c,11c] and 2) fluorine-only chemical shift or intensity imaging to track the physical transport and chemical transformation of the fluorinated probe. In the latter case, the positioning of the CF₃ group needs to be carefully considered because the lanthanide-induced pseudocontact shift is a sensitive function of molecular geometry.^[19a]

Herein, we define the theoretical framework to this approach, and in this proof-of-concept study describe the synthesis and spectroscopic properties of a series of lanthanide (III) complexes (Ln = Gd, Tb, Dy, Ho, Er, Tm) of macrocyclic ligands based on 1,4,7,10-tetraazacyclododecane (cyclen, Figure 1). We report the relaxation analysis of ¹⁹F NMR, ¹⁷O NMR and ¹H NMRD data, aided by conformational analysis using density functional theory. The charge neutral com-

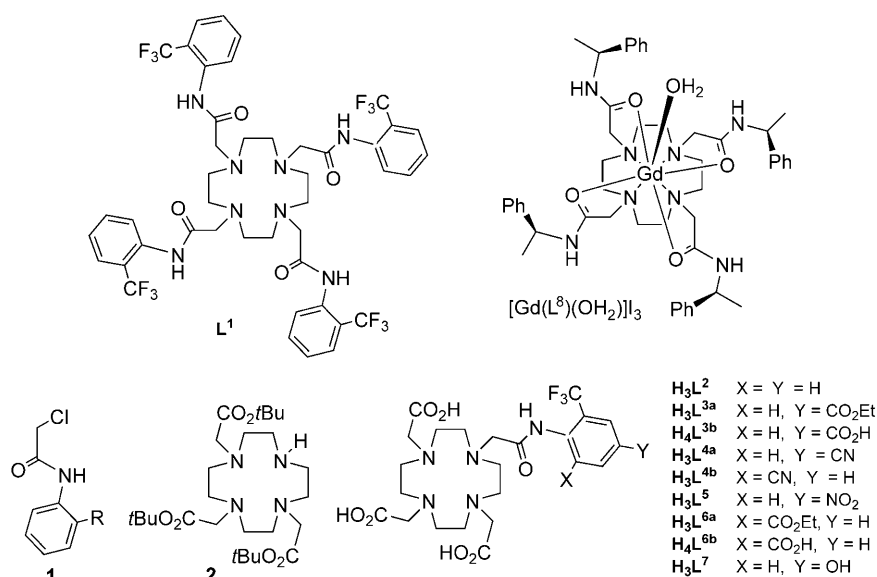


Figure 1. Structures of the ligands.

plexes selected should exhibit sufficient kinetic and thermodynamic stability to allow their safe usage in vivo.^[1,20,21] The sensitivity benefits of using such paramagnetic fluorinated probes are assessed in spectroscopic and preliminary ¹⁹F MRI experiments, as compared with a diamagnetic yttrium(III) complex.

Fluorine relaxation in paramagnetic systems: The five non-negligible spin relaxation processes for ^{19}F nuclei** in non-viscous solutions of paramagnetic molecules are due to the stochastic modulation of chemical shift anisotropy (CSA), the inter-nuclear dipole–dipole (DD) interaction, the electron–nucleus contact interaction, the electron–nucleus DD interaction and its special case known as Curie relaxation.^[22–26] Typical imaging fields are around 3.0 T, placing the systems in question firmly in the domain of perturbative spin relaxation theories,^[27–31] of which the Bloch–Redfield–Wangsness (BRW) theory^[28–30] is the one most widely used. We shall also reluctantly bow to tradition and use the isotropic tumbling approximation in the treatment below; while the more sophisticated lattice models could be desirable on theoretical grounds,^[32–39] the Lorentzian spectral density does appear to work for the small molecules reported here.

The BRW theory expressions for the CSA and inter-nuclear DD relaxation rates (ignoring the dynamic frequency shift, referring to the \hat{F}_Z state for R_1 and the \hat{F}_\pm states for R_2) are given by^[35,36]

$$R_1 = \frac{2}{15} \Delta_{\text{CSA}}^2 B_0^2 \gamma_{\text{F}}^2 \frac{\tau_{\text{R}}}{1 + \omega_{\text{F}}^2 \tau_{\text{R}}^2} \quad (1)$$

$$R_2 = \frac{1}{45} \Delta_{\text{CSA}}^2 B_0^2 \gamma_{\text{F}}^2 \left(4\tau_{\text{R}} + \frac{3\tau_{\text{R}}}{1 + \omega_{\text{F}}^2 \tau_{\text{R}}^2} \right)$$

$$R_1 = \frac{1}{10} \left(\frac{\mu_0}{4\pi} \right)^2 \sum_i \frac{\gamma_i^2 \gamma_{\text{F}}^2 \hbar^2}{r_{\text{if}}^6} \left(\frac{3\tau_{\text{R}}}{1 + \omega_{\text{F}}^2 \tau_{\text{R}}^2} + \frac{6\tau_{\text{R}}}{1 + (\omega_{\text{F}} + \omega_i)^2 \tau_{\text{R}}^2} + \frac{\tau_{\text{R}}}{1 + (\omega_{\text{F}} - \omega_i)^2 \tau_{\text{R}}^2} \right) \quad (2)$$

$$R_2 = \frac{1}{20} \left(\frac{\mu_0}{4\pi} \right)^2 \sum_i \frac{\gamma_i^2 \gamma_{\text{F}}^2 \hbar^2}{r_{\text{if}}^6} \left(4\tau_{\text{R}} + \frac{3\tau_{\text{R}}}{1 + \omega_{\text{F}}^2 \tau_{\text{R}}^2} + \frac{6\tau_{\text{R}}}{1 + \omega_i^2 \tau_{\text{R}}^2} + \frac{6\tau_{\text{R}}}{1 + (\omega_{\text{F}} + \omega_i)^2 \tau_{\text{R}}^2} + \frac{\tau_{\text{R}}}{1 + (\omega_{\text{F}} - \omega_i)^2 \tau_{\text{R}}^2} \right)$$

in which the i index runs over the nearby nuclei, B_0 is the magnetic induction, γ_{F} is the magnetogyric ratio of the fluorine nuclei, τ_{R} is the rotational correlation time and Δ_{CSA}^2 is the second invariant of the chemical shielding tensor σ with eigenvalues $\{\sigma_{\text{X}}, \sigma_{\text{Y}}, \sigma_{\text{Z}}\}$, as follows:

$$\Delta_{\text{CSA}}^2 = \begin{cases} \sigma_{\text{X}}^2 + \sigma_{\text{Y}}^2 + \sigma_{\text{Z}}^2 - \sigma_{\text{X}}\sigma_{\text{Y}} - \sigma_{\text{X}}\sigma_{\text{Z}} - \sigma_{\text{Y}}\sigma_{\text{Z}} & \text{(general case)} \\ (\sigma_{\parallel} - \sigma_{\perp})^2 & \text{(axial case)} \end{cases} \quad (3)$$

in which $\sigma_{\parallel} = \sigma_{\text{Z}}$ and $\sigma_{\perp} = \sigma_{\text{X}} = \sigma_{\text{Y}}$ in the axial case.

The electron–nuclear dipolar terms are structurally similar to the dipolar terms in Equation (2), with minor changes; the fluorine Zeeman frequency (ω_{F}) can be ignored compared with the much larger electron frequency (ω_{e}) and an

additional interaction modulation mechanism (by the electron relaxation for which $T_{1\text{e}} = T_{2\text{e}}$ is assumed) has to be included to give^[25]

$$R_1 = \frac{2}{15} \left(\frac{\mu_0}{4\pi} \right)^2 \frac{\gamma_{\text{F}}^2 g_{\text{e}}^2 \mu_{\text{B}}^2 S(S+1)}{r^6} \left(\frac{3\tau_{\text{R+e}}}{1 + \omega_{\text{F}}^2 \tau_{\text{R+e}}^2} + \frac{7\tau_{\text{R+e}}}{1 + \omega_{\text{e}}^2 \tau_{\text{R+e}}^2} \right) \quad (4)$$

$$R_2 = \frac{1}{15} \left(\frac{\mu_0}{4\pi} \right)^2 \frac{\gamma_{\text{F}}^2 g_{\text{e}}^2 \mu_{\text{B}}^2 S(S+1)}{r^6} \left(4\tau_{\text{R+e}} + \frac{3\tau_{\text{R+e}}}{1 + \omega_{\text{F}}^2 \tau_{\text{R+e}}^2} + \frac{13\tau_{\text{R+e}}}{1 + \omega_{\text{e}}^2 \tau_{\text{R+e}}^2} \right)$$

in which $\tau_{\text{R+e}} = (\tau_{\text{R}}^{-1} + T_{1\text{e}}^{-1})$. Although the point dipole approximation is not usually valid in the electron–nuclear case, the compact nature of the lanthanide f orbitals and the long (over 5 Å) electron–nucleus separation in complexes examined here make it reasonable.

The electron–nucleus contact relaxation terms are encountered in systems in which conformational mobility or electron relaxation lead to stochastic modulation of the electron–nucleus contact interaction.^[37]

$$R_1 = \frac{S(S+1)a_{\text{HFC}}^2}{3} \frac{2\tau_{\text{e}}}{1 + \omega_{\text{e}}^2 \tau_{\text{e}}^2} \quad (5)$$

$$R_2 = \frac{S(S+1)a_{\text{HFC}}^2}{3} \left(\tau_{\text{e}} + \frac{\tau_{\text{e}}}{1 + \omega_{\text{e}}^2 \tau_{\text{e}}^2} \right)$$

in which a_{HFC} is the isotropic hyperfine coupling constant, and the correlation time, τ_{e} , for its stochastic modulation is equal to the electron relaxation time. It should be noted that Equations (4) and (5) become more complicated if $T_{1\text{e}} \neq T_{2\text{e}}$.

The final relaxation mechanism, Curie relaxation, is due to the stochastic modulation of the dipole–dipole interaction between the nucleus and the static electron magnetic moment that results from the partial polarisation of the electron by the applied magnetic field.^[25] From the point of view of the nucleus, the resulting interaction is algebraically equivalent to CSA, which means that the expressions for the resulting relaxation rates, in their spectral density part, are structurally similar to those in Equation (1).

$$R_1 = \frac{2}{5} \left(\frac{\mu_0}{4\pi} \right)^2 \frac{\omega_{\text{F}}^2 g_{\text{e}}^4 S^2 (S+1)^2}{(3kT)^2 r^6} \frac{3\tau_{\text{R}}}{1 + \omega_{\text{F}}^2 \tau_{\text{R}}^2} \quad (6)$$

$$R_2 = \frac{1}{5} \left(\frac{\mu_0}{4\pi} \right)^2 \frac{\omega_{\text{F}}^2 g_{\text{e}}^4 S^2 (S+1)^2}{(3kT)^2 r^6} \left(4\tau_{\text{R}} + \frac{3\tau_{\text{R}}}{1 + \omega_{\text{F}}^2 \tau_{\text{R}}^2} \right)$$

The relatively small ligand-field splitting of lanthanide f orbitals frequently leads to more than one term being populated at room temperature, which means that the total electron angular momentum $S(S+1)$ is an effective quantity. The following (experimentally determined^[31]) parameter will be used in the treatment below:

$$\mu_{\text{eff}}^2 = g_{\text{e}}^2 \mu_{\text{B}}^2 \langle \hat{S}^2 \rangle \quad (7)$$

[**] The description below applies to most other spin- $1/2$ nuclei.

It is important to note that the five processes above do not exhaust the list of relaxation phenomena in fluorine-containing paramagnetic systems. Although the processes listed above do, in most cases, suffice, a complete description can only be claimed if the full relaxation super-operator treatment is performed^[39,40] and the system stays within the validity range of the BRW theory.

¹⁹F relaxation model for lanthanide-based MRI contrast agents

This section deals with the specific case of ¹⁹F relaxation in the lanthanide complexes reported herein. The CSA and inter-nuclear DD contributions may safely be ignored for two reasons. Firstly, on theoretical grounds, the ¹⁹F CSA in the trifluoromethyl group is quite small^[41,42] and inter-nuclear DD interaction is swamped by the much stronger electron–nuclear interactions. Secondly, from experimental observations, the fluorine *T*₁ time in diamagnetic Y³⁺ and La³⁺ complexes is about 1 s, so CSA and inter-nuclear DD cannot account for more than around 1 Hz in the measured paramagnetic relaxation rates, which are all of the order of 100 Hz. The contact mechanism may also be ruled out on theoretical grounds; a DFT calculation of isotropic hyperfine coupling between the ¹⁹F nucleus positioned over 5 Å away from the f-type unpaired electron expectedly results in a zero value.

The two remaining mechanisms (electron–nucleus DD and Curie relaxation) do contribute significantly. The resulting relaxation rates are:

$$R_1 = \frac{2}{15} \left(\frac{\mu_0}{4\pi} \right)^2 \frac{\gamma_F^2 \mu_{\text{eff}}^2}{r^6} \left(\frac{7\tau_{R+e}}{1 + \omega_e^2 \tau_{R+e}^2} + \frac{3\tau_{r+e}}{1 + \omega_F^2 \tau_{R+e}^2} \right) + \frac{2}{5} \left(\frac{\mu_0}{4\pi} \right)^2 \frac{\omega_F^2 \mu_{\text{eff}}^4}{(3kT)^2 r^6} \frac{3\tau_R}{1 + \omega_F^2 \tau_R^2} \quad (8)$$

$$R_2 = \frac{1}{15} \left(\frac{\mu_0}{4\pi} \right)^2 \frac{\gamma_F^2 \mu_{\text{eff}}^2}{r^6} \left(4\tau_{R+e} + \frac{3\tau_{R+e}}{1 + \omega_e^2 \tau_{R+e}^2} + \frac{13\tau_{r+e}}{1 + \omega_F^2 \tau_{R+e}^2} \right) + \frac{1}{5} \left(\frac{\mu_0}{4\pi} \right)^2 \frac{\omega_F^2 \mu_{\text{eff}}^4}{(3kT)^2 r^6} \left(4\tau_R + \frac{3\tau_R}{1 + \omega_F^2 \tau_R^2} \right)$$

While it is possible to make further simplifications to the above equations (extreme narrowing is sometimes assumed), we have collected sufficient data to skip further approximations and perform a direct global fit to Equations (8). As demonstrated previously,^[13] due to the presence of intermediate timescale conformational exchange, *R*₁ is a more reliable relaxation rate measure for our systems. We have, therefore, only used the *R*₁ parameter for the relaxation analyses discussed here.

Volumetric plots of the ¹⁹F relaxation rates resulting from Equations (8) are given in Figures 2 and 3, based on an idealised Ln³⁺ ion with a magnetic moment, μ_{eff} , of 10.0 Bohr magnetons (viz. Tb 9.7; Dy and Ho 10.6; Er 9.6; Tm 7.6 BM) and an electronic relaxation time of 0.20 ps. Due to the steep distance dependence of both the dipolar and Curie terms, the nuclear relaxation rates diminish fairly rapidly as the lanthanide–fluorine distance is increased. Within the

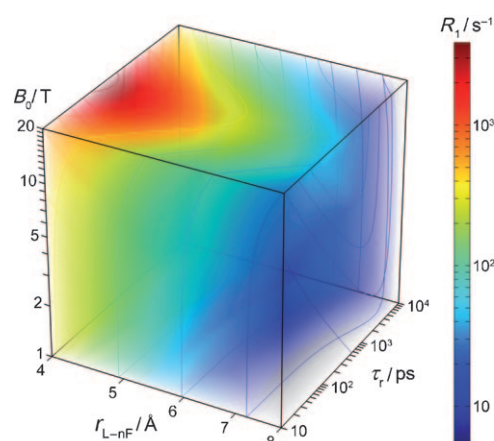


Figure 2. Volumetric plot showing the variation in *R*₁ with applied field *B*₀, mean distance *r* from the paramagnetic centre and the effective rotational correlation time, τ_r ; the analysis is based on Equation (8) and assumes $\mu_{\text{eff}} = 10$ BM with $\tau_e = 0.2$ ps.

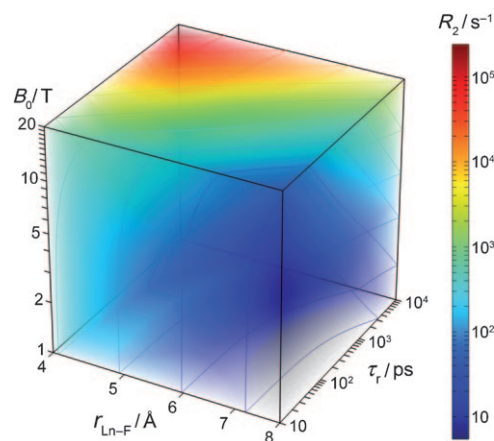


Figure 3. Volumetric plot showing the variation in *R*₂ with *B*₀, mean distance *r* from the paramagnetic centre and τ_r ; the analysis is based on Equation (8) and assumes a value of 10 BM for μ_{eff} with $\tau_e = 0.2$ ps.

typical ranges of distances, fields and correlation times, the longitudinal ¹⁹F relaxation rate has a maximum around $\omega_F^2 \tau_R^2 = 1$ and the transverse relaxation rate rises monotonously as the correlation time is increased, courtesy of the *J*(0) term in the corresponding equation.

A lanthanide complex of the type described herein (Ln = Tb, Dy, Ho, Er and Tm) possesses a τ_R value of the order of 250 ps and normally adopts a common mono-capped square anti-prismatic coordination geometry in solution.^[5,13b] At a field of 3.0 T and at a distance of between 5.5 and 6.5 Å, *R*₁ and *R*₂ values of about 100 Hz are expected. At a field of 9.4 T or above, greater line broadening is predicted for complexes of Dy, Ho and Tb and, to a lesser extent, for Er and Tm.

Complex synthesis: A series of macrocyclic ligands based on 1,4,7,10-tetraazacyclododecane, L¹–L⁷ (Figure 1) has been prepared, in which an *ortho*-trifluoromethyl group is incorporated into the phenyl ring of the amide substituent. A

DFT geometry optimisation (vide infra) gave distances of between 5 and 7 Å between the CF₃ group and the paramagnetic centre. Ligand L¹ was selected as a model complex for use in vitro, and is only for the purposes of comparison. The lower stability of the lanthanide complexes of such a tetraamide ligand precludes their safe usage in vivo. In its complexes there may be four equivalent CF₃ groups, which would lead to better ¹⁹F NMR spectroscopic sensitivity.

The lanthanide(III) complexes of monoamide derivatives of DO3A, for example, L²–L⁷, (and certain phosphinate analogues) exhibit high kinetic and thermodynamic stability with respect to metal dissociation, and hence are appropriate systems for consideration for use in vivo.^[113,36,43a] They also form several isomeric species in solution,^[43b] determined by the relative energy of stereoisomers with differing N-C-C-O (typically ±30°) and N-C-C-N (±60°) dihedral angles. Evidently, it is desirable that one major ¹⁹F resonance is observed, associated with the preferential formation of a low-energy stereoisomer.

Ligand L¹ was prepared by alkylation of cyclen with the α-haloamide **1** (MeCN, K₂CO₃), whereas ligands L²–L⁷ were obtained by stepwise alkylation of readily available ester **2**, followed by de-protection (CF₃CO₂H/CH₂Cl₂/20°C). Complex formation and purification followed standard methods by using [Ln(OAc)₃] in aqueous media (for L²–L⁷) and a Ln^{III} trifluoromethylsulfonate salt in MeCN for L^{1a}.

Spectroscopic properties: ¹⁹F NMR spectroscopic data for the complexes are reported in Table 1. For the [Ln(L¹)]³⁺ complexes,^[5,44] one major species was observed in every case, with its fraction falling in a sequence that echoed the ionic radius change, as follows: Tm (87%) > Er (85%) > Ho (75%) > Tb (70%). In each case, a second species lacking C₄ symmetry was observed, which appeared as four resonan-

ces in a 1:1:1:1 ratio. The diamagnetic complex [Y(L¹)]³⁺ gave rise to one resolved resonance, although at 656 MHz a minor species could be discerned as a shoulder. Previous crystallographic analyses of structurally related tetraamide complexes have confirmed the presence of 9-coordinate systems with one coordinated water molecule that adopt a mono-capped C₄ symmetric square antiprismatic geometry.^[45,46] The sense of the ¹⁹F pseudocontact shift (relative to the diamagnetic [Y(L¹)]³⁺ complex) follows the sign of the Bleaney coefficients;^[19a] these are negative for Tb, Dy and Ho and positive for Er, Tm and Yb. This behaviour is consistent with the adoption of a common solution structure across this series, with the CF₃ groups at a similar distance from the metal ion and subtending a similar angle to the principal axis of the complex.

For the Tb, Ho, Er and Tm complexes of ligand L²–L⁵ and L⁷, similar spectral features were noted. Immediately following dissolution of the complex in water, one main species (≥60%) was observed by using ¹⁹F and ¹H NMR spectroscopy (pD=5.4, 295 K), together with up to eight minor species that varied in relative proportion according to the nature of the Ln^{III} ion (see the Supporting Information). The ¹⁹F resonance in the corresponding Gd^{III} complexes was observed as a broad (≈1000 Hz at 295 K, 188 MHz) resonance, with a chemical shift very close to that of the analogous diamagnetic Y(III) complex (δ=−62.5 ppm), and with a longitudinal relaxation rate, R₁, of 1400 Hz (188 MHz, pD=5.4, 295 K).

Complexes of the *ortho*-substituted ligands (L^{4b}, L^{6a/6b}), for example, *ortho*-ester L^{6a} and derived carboxylate L^{6b}, behaved very differently. For each Ln^{III} complex of L^{6a}, two species separated by δ=49.7 (Tb), 33.4 (Ho), 20.0 (Er) and 53.6 ppm (Tm) were observed in a 1:1 ratio. For [Ln(L^{6b})], the two species were present in a 3:1 ratio with very similar ¹⁹F shifts to the ester series (Table 1) but with much greater linewidths. The europium emission spectra for the ester and acid complexes were identical in form and were the same at pH 5 and 8. Measurements of the radiative lifetime of the europium excited state, *k*, were made in H₂O and D₂O to allow assessment of the complex hydration state. Values of *k* for [Eu(L^{6a})] were 1.84 (H₂O) and 0.54 ms^{−1} (D₂O); for [Eu(L^{6b})] the corresponding values were 1.70 and 0.60 ms^{−1}. This data is consistent with europium hydration states, *q*, of 1.2 and 0.9, respectively. The common hydration state and the absence of change in the form and relative intensity of the Eu emission spectra strongly suggests that a common metal coordination environment is adopted in solution in each case, with no evidence for carboxylate ligation to Eu.

A variable-temperature ¹H NMR spectroscopic study of both [Tm(L^{6a})] and [Tm(L^{6a})][−] was carried out at pH 5 (D₂O insert, 470 MHz) over a temperature range of 283 to 323 K. For the ester complex, the observed linewidth of each resonance increased with increasing temperature. At 293 K the linewidth was 70 Hz and at 323 K each resonance had a linewidth of 600 Hz, but there was less than a δ=5 ppm change in the chemical shift. For [Tm(L^{6b})][−], the two resonances shifted and broadened as *T* increased and a coa-

Table 1. ¹⁹F NMR chemical shift data [ppm] for lanthanide(III) complexes (295 K, pD=5.4, Ln=Tb, Ho, Er, Tm, Dy).^[a,b]

Complex	Tb	Ho	Er	Tm	Dy
[Ln(L ¹)] ^[c,d]	−53.9	−59.0	−63.5	−65.1	
[Ln(L ²)] ^[e,f]	−51.9 (−36.7)	−64.2 (−50.8)	−64.8 (−70.4)	−77.4 (−66.8)	
[Ln(L ^{3a})]	−49.3	−56.8	−62.4	−78.1	−64.3
[Ln(L ^{3b})]	−51.2	−57.1	−62.0	−79.2	−65.0
[Ln(L ^{4a})]	−50.1	−55.4	−64.1	−78.2	
[Ln(L ^{4b})] ^[f]	−84.6 (−40.6)	−78.1 (−48.8)	−49.6 (−67.6)	−39.0 (−88.1)	
[Ln(L ⁵)]	−50.1	−55.1	−64.7	−77.5	−58.3
[Ln(L ^{6a})] ^[f]	−89.0 (−39.3)	−82.9 (−49.5)	−49.7 (−69.7)	−38.0 (−91.6)	
[Ln(L ^{6b})] ^[f]	−90.4 (−42.1)	−79.3 (−46.4)	−45.8 (−66.6)	−35.4 (−88.7)	
[Ln(L ⁷)] ^[f]	−52.5 (−40.6)	−57.9 (−49.0)	−63.4 (−68.9)	−78.1 (−89.2)	−66.7

[a] The ligands each have a chemical shift of δ=(−61.6±0.5) ppm under these conditions. [b] The corresponding Gd^{III} complexes give rise to very broad resonances at δ_F=(−62±2) ppm, ω_{1/2}=3000 Hz at 4.7 T. [c] In 80% CD₃OD/D₂O. [d] Only one species was observed at δ=−62.5 ppm. [e] The major species was observed at δ=−61.0 ppm. [f] Values in parenthesis refer to the second most abundant species (ratios are 1:1 for [Ln(L^{4b})] and for [Ln(L^{6a}/L^{6b})], the ratios are 1:1 and 3:1).

lescence phenomenon was observed at 320 K. The major resonance was observed at $\delta = -84$ ppm ($\omega_{1/2} \approx 1800$ Hz). Evidently, these conformers ($\Delta\nu = 24,500$ Hz) are in dynamic exchange on the NMR timescale, with an activation energy of the order of 50 kJ mol^{-1} , based on a simple Eyring analysis. Further information on this process and the nature of these isomers was obtained in computational DFT studies (vide infra).

Protonation equilibria: The nature of the substituents of the aromatic ring in ligands L^1 – L^7 determines the pK_a of the amide hydrogen and thereby the pH sensitivity of the observed NMR chemical shift. Complexes of L^1 , L^2 and L^7 , which have H or an OH group in the *para* position, showed no variation in the ^{19}F chemical shift at pH values between 3.5 and 8.0, consistent with a pK_a of ≥ 9.5 . For each of the Ln^{III} complexes of L^3 – L^6 , the chemical shift of the CF_3 group changed markedly between pH 6 and 10 (Table 2 and Figure 4). Because the acid–base equilibrium is fast on the

Table 2. Chemical shift [ppm] and linewidth [Hz] data (295 K, 188 MHz, H_2O , D_2O capillary lock, 1 mm) for Ln^{III} complexes of L^5 and L^{4a} ($pK_a = (7.77 \pm 0.03)$ and (7.81 ± 0.03) , respectively).

Complex	pH 5		pH 9	
	δ_{F}	$\omega_{1/2}$	δ_{F}	$\omega_{1/2}$
[Tb(L^5)]	-50.2	73	-26.4	366
[Ho(L^5)]	-55.4	39	-36.8	340
[Er(L^5)]	-64.7	63	-74.5	120
[Tm(L^5)]	-77.5	45	-89.6	277
[Tb(L^{4a})]	-50.1	63	-32.8	150
[Tb(L^{4b})]	-40.6	500	-3.9	190
	-84.6		-73.1	
[Ho(L^{4a})]	-55.4	45	-42.5	125
[Ho(L^{4b})]	-48.8	420	-25.6	195
	-78.1		-68.8	
[Er(L^{4a})]	-64.1	39	-72.2	95
[Er(L^{4b})]	-49.6	425	-53.1	190
	-67.6		-81.6	
[Tm(L^{4a})]	-78.2	36	-87.6	99
[Tm(L^{4b})]	-39.0	420	-39.9	195
	-88.1		-109.0	

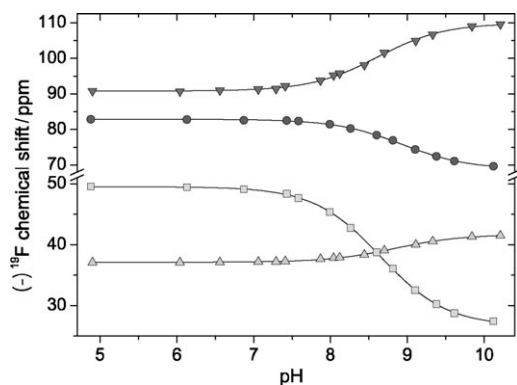


Figure 4. Variation in δ_{F} with pH for each isomer of $[\text{Ho}(\text{L}^{6a})(\text{OH}_2)]$ (Ho^{3+} (major form): \blacksquare and Ho^{3+} (minor form): \bullet), and $[\text{Tm}(\text{L}^{6a})(\text{OH}_2)]$ (Tm^{3+} (major form): \blacktriangledown and Tm^{3+} (minor form): \blacktriangle). Conditions: 295 K, H_2O with D_2O capillary, 0.1 M NaCl.

NMR timescale, only one signal was usually observed, which corresponds to the weighted average of the chemical shifts of the amide and its conjugate base. The pK_a associated with deprotonation of the amide NH, follows the sequence $o\text{-CN} < p\text{-NO}_2 \approx p\text{-CN} < p\text{-CO}_2\text{Et} < o\text{-CO}_2\text{Et} < p\text{-CO}_2^- \ll o\text{-CO}_2^-$. This order reflects the combined effects of the electronegativity of the substituent and Coulombic repulsion, and correlates well with published pK_a values for the ionisation of related substituted phenols.

The two major isomers of complexes of the *ortho*-cyano ligand, $[\text{Ln}(\text{L}^{4b})]$, exhibit a large change in chemical shift associated with amide NH deprotonation at around pH 7; for example, the pK_a for $[\text{Ho}(\text{L}^{4b})]$ is 7.0 (Figure 5). The chemi-

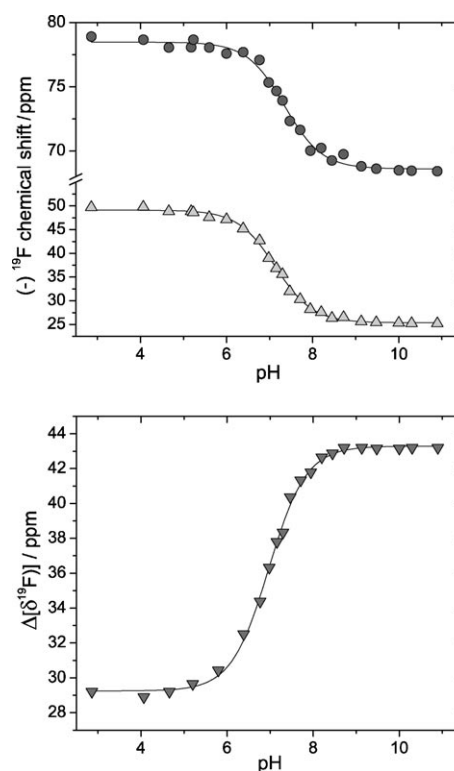


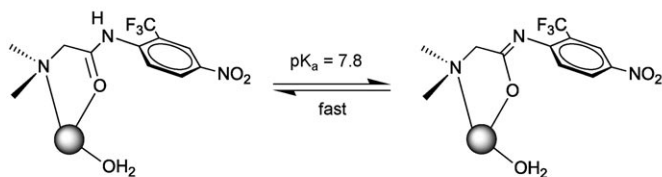
Figure 5. Top: Variation in δ_{F} with pH for each isomer of $[\text{Ho}(\text{L}^{4b})(\text{OH}_2)]$ (\blacktriangle and \bullet represent the two isomers present in a ratio of 1:1 at room temperature). Bottom: The difference in chemical shift between the isomers due to the variation in pH. Conditions: 295 K, H_2O with D_2O capillary, 0.1 M NaCl; pK_a 7.0.

cal shift of each isomer exhibits a different sensitivity to pH, so that the shift difference between the two species allows a simple means of determining the pH. This is a very attractive method for determining pH because no chemical shift referencing is required and the pK_a value of 7.0 is very well suited to studies in biological media.

In certain cases (e.g., $[\text{Ho}(\text{L}^5)]^-$), the ^{19}F NMR linewidth of the conjugate base is significantly broader, by about a factor of eight, than the protonated amide $[\text{Ho}(\text{L}^5\text{H})]$. At higher temperatures, the linewidth decreased considerably. Such behaviour is consistent with the presence of an intermediate timescale conformational exchange in the deproton-

ated complex. This tendency was most pronounced for [Ho(L⁵)] and [Tb(L⁵)], and was less apparent with [Er(L⁵)] or [Tm(L⁵)], (see the Supporting Information). For the *para*-substituted analogues, [Ln(L^{3a})] (*p*-CO₂Et) and [Ln(L⁴)] (*p*-CN), somewhat different behaviour was observed for the variation in the linewidth with pH. In these cases, the linewidth reached a maximum at the pK_a and decreased to a lower value as the pH was raised further. The exchange broadening observed in these cases presumably relates to the effect of chemical exchange between the amide and its conjugate base.

Two different chemical exchange processes can be considered to account for the extensive line broadening, most clearly exemplified with the conjugate base for [Ho(L⁵)]⁻ and [Tb(L⁵)]⁻. These involve either a lanthanide re-coordination from O to N or a *cis*–*trans* isomerisation around the carbon–nitrogen double bond. We reported in a preliminary communication that extended DFT calculations could be used^[13b] to assess the likelihood of these processes. Lanthanide re-coordination was ruled out because the calculated energy difference between O- and N-coordinated constitutional isomers was 62 kJ mol⁻¹ in favour of the O-bound isomer. The calculated energy difference between the *cis* and *trans* isomers was 18 kJ mol⁻¹, and calculated activation energies for the forward and backward isomerisation reactions were computed to be 27 and 45 kJ mol⁻¹, respectively. Therefore, the isomerisation process depicted in Scheme 1 offers a reasonable explanation, with preferred conformers placing the bulky CF₃ group away from the amide oxygen.



Scheme 1. Protonation and conformational equilibria in [Ln(L⁵)].

Relaxation analysis: ¹⁹F longitudinal relaxation rates were measured by using the inversion-recovery technique (without proton decoupling) in dilute (1.0 mM) solutions in D₂O (pD=5.4; D₂O used for lock) at 295 K. Inversion-recovery type function was fitted to the resulting data by using Levenberg–Marquardt minimisation of the non-linear least squares error functional. The resulting relaxation rates (Tables 3 and 4) follow the order: Dy > Tb > Ho > Er > Tm, consistent with the presence of μ_{eff}² and μ_{eff}⁴ terms in Equa-

Table 3. ¹⁹F longitudinal relaxation rates for [Ln(L¹)]Cl₃ and [Ln(L^{6a})] (295 K, pD=5.4, D₂O).^[a]

Ln	[Ln(L ¹)] ³⁺				[Ln(L ^{6a})] ^[b,c]			
	4.7 T	9.4 T	11.7 T	16.5 T	4.7 T	9.4 T	11.7 T	16.5 T
Tb	115 ± 2	185 ± 4	224 ± 3	282 ± 8	149 100	250 147	323 179	565 192
Ho	84.0 ± 2.0	192.1 ± 1.5	249.6 ± 2.6	340.8 ± 7.5	91 ± 1 71 ± 1	233 ± 2 137 ± 2	333 ± 4 172 ± 3	588 ± 15 313 ± 8
Er	45.8 ± 0.3	108.7 ± 1.0	143.3 ± 0.3	199.5 ± 0.7	59.0 ± 0.5 45 ± 1	152.0 ± 1.2 88 ± 1	208.5 ± 2.5 110 ± 2	313 ± 6 161 ± 3
Tm	33.0 ± 0.6	59.7 ± 1.3	76.2 ± 0.4	102.3 ± 0.4	53 37	100 56	135 68	294 152

[a] For [Y(L¹)]Cl₃, R₁ = 0.78 ± 0.03 s⁻¹ and R₂ = 2.9 ± 0.2 s⁻¹. [b] Values for [Ln(L^{6a})] refer to the two major conformers that are in slow exchange on the NMR time-scale. [c] For [Ln(L^{6b})], the two major species observed are in intermediate exchange so that the same or similar R₁ values are observed, notably at lower field.

Table 4. ¹⁹F relaxation parameters [Hz] for [Ln(L⁷)] (295 K, pD=5.4, D₂O).^[a]

magnetic field [T]	Tb ^[b,c]		Dy ^[b,c]		Ho ^[b,c,d]		Er ^[b,c]		Tm ^[b,c]	
	R ₁	R ₂	R ₁	R ₂	R ₁	R ₂	R ₁	R ₂	R ₁	R ₂
4.7	74 ± 6	124	89 ± 8	156	45.5 ± 2.5	87	34 ± 2	120	22.9 ± 0.5	53
9.4	133 ± 7	206	162 ± 11	355	124 ± 10	192	75 ± 3	198	47 ± 7	89
11.7	161.7 ± 0.5	271	201 ± 13	543	169 ± 19	267	102.5 ± 0.7	251	57.5 ± 0.5	112
16.5	211.1 ± 0.5	407	286 ± 13	740	238.7 ± 1.6	441	144 ± 2	317	74.4 ± 0.5	168

[a] In these complexes, the CF₃ group is estimated to be (6.9 ± 0.8) Å from the Ln^{III} ion if a global fitting analysis of all data sets is used, or (6.24 ± 0.02) Å, if literature μ_{eff} data is used in the calculation (see text). [b] The estimated standard deviations for R₁ are given. [c] R₂ values were estimated as (πω_{1/2}) for a Lorentzian line fit. [d] The R₁ data at 4.7 T for related Ho^{III} complexes was similar: [Ho(L²)] 48 s⁻¹, [Ho(L^{3a})] 55 s⁻¹, [Ho(L^{3b})]⁻ 50 s⁻¹, [Ho(L⁴)] 42 s⁻¹, [Ho(L⁵)] 40 s⁻¹. Similar trends were observed for the Tb(III), Er(III) and Tm(III) complexes of L²–L⁵.

tions (8). For a given lanthanide, the relaxation rates drop in the sequence [Ln(L^{6a})] > [Ln(L¹)]³⁺ > [Ln(L⁷)], which suggests that the distance between the CF₃ group and the paramagnetic centre also decreases in this order. For the *para*-substituted analogues of [Ln(L⁷)], that is, [Ln(L²)]–[Ln(L⁵)], the measured relaxation rates were found to be very similar.

To extract the average Ln–F lengths and rotational correlation times from the field dependence of the longitudinal relaxation rate, a global non-linear least-squares fit was performed for Equation (8). It was assumed that the Ln–F length and the rotational correlation time remain the same in the {Dy, Tb, Ho, Er, Tm} sequence (which makes *r* and τ_R

global variables). This is reasonable because the ionic radius variation in this series is minor.^[47] The values of μ_{eff} and τ_e were kept local for every lanthanide. While each individual fit is ambiguous, the global fit (Figure 6) has a single, well-

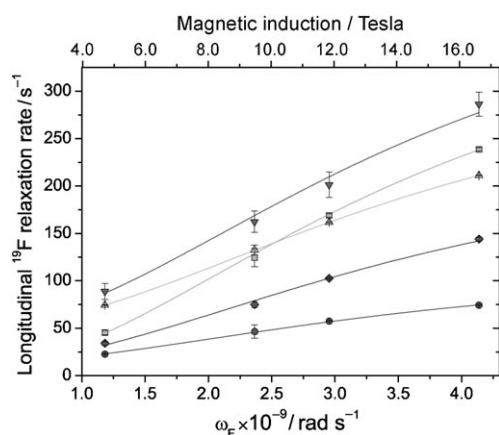


Figure 6. Variation in R_1 with ω_F for $[\text{Ln}(\text{L}^7)(\text{OH}_2)]$ ($\text{Ln}=\text{Tb}$ (\blacktriangle), Dy (\blacktriangledown), Ho (\blacksquare), Er (\blacklozenge) and Tm (\bullet); 295 K, 1 mm). The solid lines represent the global least-squares fit to Equation (8). The steeper rise of the Ho curve as a function of magnetic field is due to its shorter electron relaxation time compared with the other lanthanides.

defined weighted least-squares minimum that results in $\tau_R=270\pm 10$ ps, $r=6.3\pm 0.7$ Å and the effective magnetic moments in Table 5. A Stokes–Einstein estimate by using DFT molecular geometry in D_2O at 298 K gives $\tau_R=272$ ps

Table 5. Experimental values of μ_{eff} [BM].

Ln	Values from refs. [5,19]	Measured
Tb	9.7	9.8 ± 1.8
Dy	10.6	10.6 ± 1.9
Ho	10.6	10.4 ± 1.9
Er	9.6	9.1 ± 1.6
Tm	7.6	7.6 ± 1.4

($\langle r_{\text{mol}} \rangle = 6.18$ Å), with a DFT-calculated Ln–F length of $\langle r \rangle = 6.95$ Å. Slightly lower values of τ_R that had been reported to come from ^1H NMRD spectroscopic analyses of structurally related complexes^[48] are probably the consequence of the fact that ^1H NMRD spectroscopy implicitly examines the motion of the Ln–(water proton) vector, whereas the analysis above refers to the Ln–F vector. Another possible factor is the fact that the viscosity of D_2O is 20% higher than H_2O .

Similar global fitting analyses of the R_1 data at different fields (Table 3) were also carried out for the Tb, Ho, Er and Tm complexes of L^1 and L^{6a} . For $[\text{Ln}(\text{L}^1)(\text{OH}_2)]^{3+}$, the Ln–F length was estimated to be 6.1 ± 0.2 Å, with a rotational correlation time of 255 ± 20 ps. For the *ortho*-ester complexes, $[\text{Ln}(\text{L}^{6a})(\text{OH}_2)]$, ^{19}F NMR spectroscopy revealed the presence of two isomeric species in solution in approximately 1:1 ratio (not changing significantly between the different lanthanides examined). The value of the distance, r , for each

species was found to be 5.7 ± 0.1 Å and 6.3 ± 0.2 Å with a τ_R value of 243 ± 23 ps (Figure 7a). DFT calculations on this system gave values for the distance (linear average over the three fluorine atoms) of 5.6 Å and 6.2 Å. A τ_R value of 300 ps was estimated by using the Stokes–Einstein equation

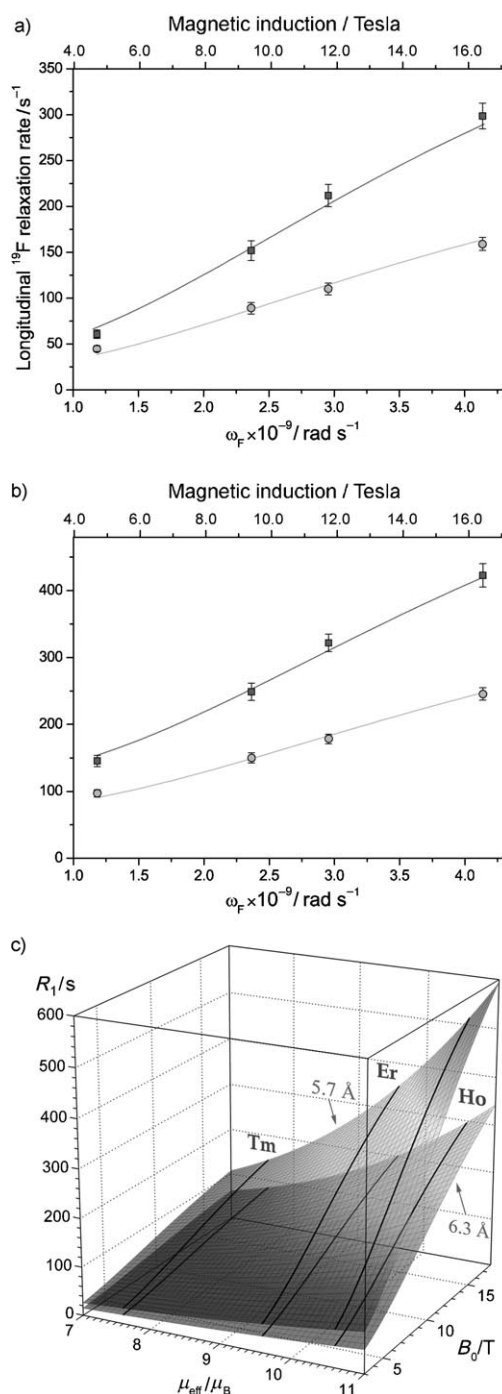


Figure 7. Variation in R_1 with ω_F for the two major isomers of a) $[\text{Er}(\text{L}^{6a})(\text{OH}_2)]$ (\blacksquare : $\text{Er}(\text{L-COOEt})\text{-A}$, \bullet : $\text{Er}(\text{L-COOEt})\text{-B}$) and b) $[\text{Tb}(\text{L}^{6a})(\text{OH}_2)]$ (\blacksquare : $\text{Tb}(\text{L-COOEt})\text{-A}$, \bullet : $\text{Tb}(\text{L-COOEt})\text{-B}$); conditions: 295 K, 1 mm. The solid lines represent the global least-squares fit to Equation (8). c) Calculated volumetric plot showing the variation in R_1 with B_0 and μ_{eff} for $r=5.7$ and 6.3 Å. The rotational correlation time, τ_R is fixed at 250 ps and $\tau_e=0.2$ ps is assumed; the analysis is based on Equation (8).

from the DFT molecular volume (effective molecular radius of 6.6 Å).

Using the approach defined above for the volumetric plots (Figures 2 and 3), the variation of R_1 with μ_{eff} and B_0 can be calculated by using the experimental distance values of 5.7 and 6.3 Å. This analysis, based on $\tau_{\text{R}}=250$ ps and $\tau_{\text{e}}=0.2$ ps, generates two surfaces (Figure 7b), which highlight the steeper increase in R_1 at higher fields for the Er and especially the Ho complex.

It appears that, in designing a fluorinated paramagnetic probe, to avoid very high relaxation rates (and hence much broader lines) the CF_3 group should be no closer than 5.5 Å from the Ln ion in Ho and Er complexes, and by inference the Tb/Dy analogues. Thulium complexes would be more useful if higher magnetic fields are used. On the other hand, Tb, Dy and Ho complexes relax the CF_3 group efficiently at a distance of about 6 Å and over the field range of 3 to 7 T and should, therefore, allow rapid acquisition of signal intensity without undue line broadening and the associated sensitivity issues.

Conformational analysis: The DFT calculations were performed by using the Gaussian 03^[55] package for La^{3+} and Y^{3+} complexes; the structures of complexes with other lanthanides are likely to be nearly identical to the Y^{3+} complex. The Y^{3+} results were very similar to those obtained with La^{3+} , and given the similarity (± 0.02 Å) of the ionic radii of Ho^{3+} , Y^{3+} and Er^{3+} , only the Y^{3+} complex computations are described herein.

^{19}F NMR spectra reported for $[\text{Ln}(\text{L}^{6a})]$ and $[\text{Ln}(\text{L}^{6b})]$ and for the *ortho*-cyano series $[\text{Ln}(\text{L}^{4b})]$ show two major signals of comparable intensity but with very different chemical shifts, which suggests a conformational equilibrium between two states with very different positions of the CF_3 group with respect to the pseudocontact shift field of the complex. The observed slow rate of chemical exchange also indicates a large activation energy for the transition between the two conformers.

A very likely candidate for the conformational transition in question is the variation of the C-N-C-C dihedral angle that results in the phenyl ring flip and consequent repositioning of the CF_3 group relative to the metal centre. To confirm this hypothesis, a relaxed potential energy scan was performed with respect to the C-C-N-C dihedral angle for the Y^{III} analogue of complexes involving ligands $\text{L}^4\text{-L}^{6a}$. In each case, two distinct minima were indeed identified (Figure 8), separated by an energy barrier of >20 kJ mol⁻¹ and featuring very different positions of the CF_3 reporter group with respect to the metal centre. Taking the metal-water-oxygen vector to be the principal axis, the CF_3 groups are oriented at angles of -114° and $+44^\circ$, respectively, in each isomer. In the axial PCS case, these angles would give rise to opposite pseudocontact shifts. The calculated $\text{Y}_{2,0}$ spherical harmonic terms for the angles of -114 and $+44^\circ$ are -0.50 and $+0.55$. For the Ho complex, ^{19}F chemical shifts of $\delta = -82.9$ and -49.5 ppm were measured (Table 1). For the thulium analogue, the corresponding values were

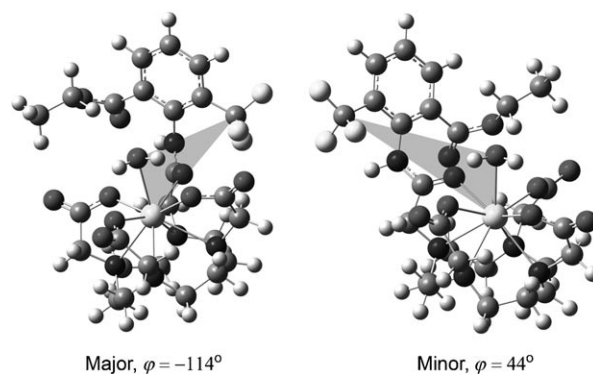


Figure 8. DFT-calculated structures showing the two low-energy isomers of $[\text{Ln}(\text{L}^{6a})(\text{OH}_2)]$ that arise from rotation about the aryl-N bond.

$\delta = -38.0$ and -91.6 ppm compared with $\delta = -62$ ppm for the diamagnetic yttrium complex. Given that the Bleaney coefficients^[19a] for Ho and Tm are -39 and $+53$ (relative to Dy at -100), the sense and size of the observed shifts agrees well with the expected values and lends support to the hypothesis of the two low-energy conformers identified by the DFT calculation (Figure 8).

Relaxation properties of gadolinium(III) complexes: The gadolinium complexes of these ligands can also be used as conventional contrast agents for proton MRI by enhancing the rate of relaxation of the bulk water signal. Therefore, the proton relaxation behaviour of selected examples was also characterised. It should be noted that only the mono-amide derivatives are likely to be useful in vivo because the tetraamide examples reported here possess limited water solubility and have much lower kinetic stability with respect to metal dissociation, precluding their safe use in vivo.

In aqueous solution, mono-aqua gadolinium(III) complexes of a variety of acyclic and macrocyclic octadentate ligands efficiently catalyse the relaxation of the bulk water ^1H NMR signal.^[5] The measured relaxation rate of water, R_1 , in the presence of a gadolinium complex is made up of diamagnetic and paramagnetic terms, of which the latter set comprises contributions from inner (*is*), second-sphere (*ss*) and outer-sphere water (*os*) molecules, [Eqns (9)–(11)]. The increment of the paramagnetic contribution to the water proton relaxation rate per unit concentration is termed the relaxivity, r_{1p} , of the complex.

$$R_1 = R_{1d} + R_{1p} = R_{1d} + R_1^{is} + R_1^{ss} + R_1^{os} \quad (9)$$

$$r_{1p} = R_{1p}/[\text{Gd}(\text{L})] \quad (10)$$

$$R_{1p}^{is} = \frac{[\text{Gd}(\text{L})]q}{55.6(T_m + \tau_m)} \quad (11)$$

For low-molecular-weight Gd complexes, the inner-sphere contribution often dominates and is approximated by Equation (11), in which τ_m is the mean water residence lifetime (at Gd), q is the number of coordinated water molecules

and T_{1m} is the longitudinal relaxation time of the coordinated water protons. If water exchange is slow ($\tau_m > T_{1m}$), then the measured relaxivity may tend to a lower limit in which only the second-sphere and outer-sphere terms contribute.^[17,49–51]

In the case of $[\text{Gd}(\text{L}^1)(\text{OH}_2)]\text{Cl}_3$, the limited water solubility of this complex precluded accurate measurements of the temperature dependence of the transverse relaxation rate of the ^{17}O water signal. For each of the other complexes examined, variable-temperature ^{17}O NMR measurements were undertaken with 19 to 32 mM solutions of the complex in ^{17}O -enriched water and the data were analysed by using standard Swift–Connick methodology^[52] to give estimates of the water exchange lifetime, τ_m . Values of τ_m for $[\text{Gd}(\text{L}^2)(\text{OH}_2)]$ and $[\text{Gd}(\text{L}^{6a}/\text{L}^{6b})(\text{OH}_2)]$ fell in the range of 0.5 to 1.0 μs , typical of a variety of related monoamide derivatives of $[\text{Gd-DO3A}]$.^[5] For $[\text{Gd}(\text{L}^1)(\text{OH}_2)]\text{Cl}_3$, information on the water exchange rate was extracted by analysing the temperature dependence of r_{1p} (as detailed in reference [42]) in association with classical analyses of the field dependence of relaxivity (0.01 to 70 MHz (Figure 9), based on the Solomon–Bloembergen–Morgan equations that rationalise the time dependence of the water proton– Gd^{III} dipolar coupling with the added consideration of the second-sphere contribution.^[5,17] It is appreciated that these models have their limitations, but the analysis used here adopts this approach to allow comparison with similarly derived literature data.

The proton relaxivity of $[\text{Gd}(\text{L}^{1a})(\text{OH}_2)]\text{Cl}_3$ was $6.5 \text{ mM}^{-1} \text{ s}^{-1}$ (20 MHz, 298 K) and decreased as a function of temperature, (Figure 9), consistent with relatively fast water exchange at the Gd^{3+} centre ($\tau_m = 3.5 \mu\text{s}$). This behaviour is

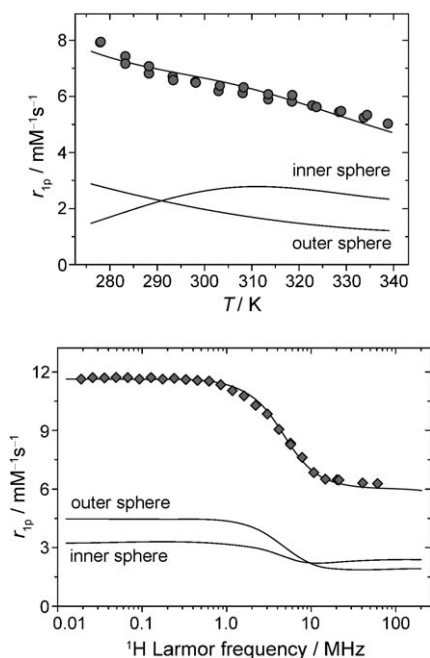


Figure 9. Variation in the relaxivity (r_{1p}) of $[\text{Gd}(\text{L}^1)(\text{OH}_2)]\text{Cl}_3$ with a) temperature and b) field showing the estimated contributions of inner- and outer-sphere waters.

in marked contrast to structurally related tetraamide complexes, such as $[\text{Gd}(\text{L}^8)(\text{OH}_2)]\text{X}_3$, for which the measured relaxivity was $2.3 \text{ mM}^{-1} \text{ s}^{-1}$ (20 MHz, 298 K). They exhibit a markedly different temperature dependence (Figure 10) associated with a very long water exchange lifetime ($\tau_m \approx 100 \mu\text{s}$) that is independent of the nature of X (X = Cl, Br,

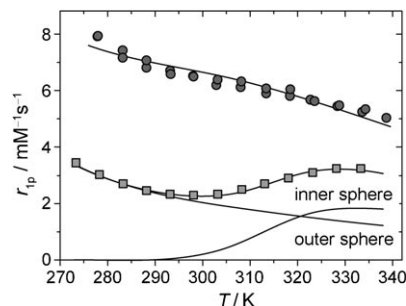


Figure 10. Comparison of the variation in the relaxivity (r_{1p}) of $[\text{Gd}(\text{L}^1)(\text{OH}_2)]\text{Cl}_3$ (\bullet) with $[\text{Gd}(\text{L}^8)(\text{OH}_2)]\text{Cl}_3$ (\blacksquare); the lower inner-sphere contributions have been highlighted in the latter case due to slow water exchange (τ_m of ca. 100 μs).

I, OAc, NO_3).^[49] The long τ_m values for $[\text{Gd}(\text{L}^8)(\text{OH}_2)]\text{X}_3$ are associated with a high activation enthalpy (Table 6) of the order of 120 kJ mol^{-1} . This contrasts with the value of 30 kJ mol^{-1} estimated for $[\text{Gd}(\text{L}^1)(\text{OH}_2)]\text{Cl}_3$. Such behaviour is consistent with the presence of a highly hydrophobic environment around the coordinated water in $[\text{Gd}(\text{L}^8)(\text{OH}_2)]^{3+}$ salts, that suppresses the water interchange process. Evidently there must be a more open structure in the $[\text{Gd}(\text{L}^1)(\text{OH}_2)]^{3+}$ complex, with a well-defined second-sphere of hydration that assists the water interchange at gadolinium.

The relaxivity of $[\text{Gd}(\text{L}^2)(\text{OH}_2)]$ and $[\text{Gd}(\text{L}^{6a}/\text{L}^{6b})(\text{OH}_2)]$ was independent of pH ($\pm 7\%$) over the pH range of 2.5 to 11.5 and did not vary significantly over a 24 h time period, consistent with high kinetic stability with respect to acid-catalysed or base-promoted dissociation pathways. There were subtle differences in the relaxation parameters for the ester, $[\text{Gd}(\text{L}^{6a})(\text{OH}_2)]$ and the derived carboxylate $[\text{Gd}(\text{L}^{6b})(\text{OH}_2)]^-$ (Table 6). The relaxivity and τ_r values of the ester complex were slightly higher and the water exchange lifetime was slightly lower. These variations are likely to reflect small changes in the second sphere of hydration. For example, in $[\text{Gd}(\text{L}^2)(\text{OH}_2)]$ and $[\text{Gd}(\text{L}^{6a})(\text{OH}_2)]$ the amide NH can act as a hydrogen-bond donor to a proximate water molecule. This tendency is likely to be suppressed for $[\text{Gd}(\text{L}^{6b})(\text{OH}_2)]^-$ because it can adopt a low-energy conformation that involves an intramolecular hydrogen bond between the carboxylate anion and the amide NH proton.

Sensitivity enhancement in spectroscopic and preliminary ^{19}F imaging studies: A comparative study was undertaken to assess the gain in signal intensity for Tb, Ho and Er complexes of L^3 over the diamagnetic Y analogue. Equimolar solutions were used and spectral signal intensity recorded at

Table 6. Summary of selected relaxation parameters (298 K) derived from analysis of variable-temperature ^1H relaxivity, ^{17}O NMR spectroscopy and fitting of NMRD profiles.^[a]

	$[\text{Gd}(\text{L}^1)(\text{OH}_2)]\text{Cl}_3$	$[\text{Gd}(\text{L}^8)(\text{OH}_2)]\text{I}_3$ ^[b]	$[\text{Gd}(\text{L}^2)(\text{OH}_2)]$	$[\text{Gd}(\text{L}^{6a})(\text{OH}_2)]$	$[\text{Gd}(\text{L}^{6b})(\text{OH}_2)]^-$
r_{1p} [$\text{mM}^{-1}\text{s}^{-1}$]	6.5	2.3	5.5	5.4	4.95
τ_m [μs]	3.5	101	0.90	0.57	0.93
τ_R [ps] ^[c]	118	103	88	81	81
τ_r [ps]	13	8	14	15	13
$\Delta^2 \times 10^{19}$ [s^{-2}]	4.0	1.5	5.9	6.3	6.3
ΔH_m [kJ mol^{-1}]	30.1	117	48.0	38.9	33.7
ΔH_r [kJ mol^{-1}]	16	14	18	18	18
ΔH_s [kJ mol^{-1}]	2.0	5.0	2.0	3.0	2.0
q ^[d]	1	1	1	1	1
ΔH_d [kJ mol^{-1}]	-22	-25	-24	-25	-25
q''	8	0	2	2	2
r'' [\AA]	4.4	n/a	4.4	4.3	4.5

[a] The Gd–H distances for the coordinated water molecule (r) and the outer-sphere water molecules (a) were fixed to the standard values of 3.0 and 4.0 \AA . The value of $2.24 \times 10^{-5} \text{ cm}^2 \text{ s}^{-1}$ (298 K) was used for the relative diffusion coefficient between solute and solvent molecules. [b] The chloride salt of $[\text{Gd}(\text{L}^8)]$ gave identical q , relaxivity, τ_m and τ_R values.^[49] [c] Values of τ_R derived by analysis of NMRD profiles or r_{1p}/T variations will tend to underestimate τ_R ^[3,13b] because they implicitly analyse the motion of the Gd–OH₂ moiety, which may not correlate well with the overall tumbling motion of the complex. Values of τ_R derived from analysis of the relaxation times of $^2\text{H}/^{13}\text{C}$ -labelled ligands always give higher estimates.^[48] [d] The values of q were confirmed by analysis of emission lifetime data^[53] for analogous Tb complexes, e.g., $[\text{Tb}(\text{L}^1)]\text{Cl}_3$, $k_{\text{H}_2\text{O}}=0.57$, $k_{\text{D}_2\text{O}}=0.31$, $q=1.0$ (± 0.1).

9.4 T with an acquisition time of three times the measured T_1 value, and spectral data was acquired for 20 min in each case. The values obtained (Table 7) reveal the expected gains in signal intensity, which are of the order of a factor of 10.

Table 7. Assessment of ^{19}F NMR spectroscopic sensitivity.^[a]

	Acquisition time ^[b] [s]	Number of transients	Relative signal intensity ^[c,d]
$[\text{Y}(\text{L}^2)]$	2.346	496	1
$[\text{Tb}(\text{L}^2)]$	0.034	32 688	25
$[\text{Ho}(\text{L}^2)]$	0.029	38 464	7
$[\text{Er}(\text{L}^2)]$	0.075	15 536	10

[a] For 2 mm samples at 188 MHz and 293 K. [b] The acquisition time was set as $3 \times T_1$, with no delay time; in spectral processing the line broadening was set as 50% of the observed linewidth in each case. [c] Relative signal intensity was scaled in proportion to the mole fraction of the major isomer. [d] With no line-broadening function applied, the order of signal intensity (as above) was 1:44:33:29.

A preliminary imaging study was carried out at 7 T. R_1 values were estimated to be 77.8 s^{-1} and 0.8 s^{-1} for the Ho and Y complexes of L^3 , which leads to Ernst angles^[54] of 78° and 13° , respectively, for a 20 ms repetition rate, T_R . Fluorine MR images of equimolar solutions of the samples were collected (Figure 11) with 768 averages and a total data collection time of 16.5 min. The signal-to-noise ratio in the Ho complex was 10.7 compared with 4.4 in the yttrium complex, which gives a sensitivity improvement of 2.4 compared with the theoretical sensitivity difference of 5.7 for Ernst angle imaging under these conditions. Although the minimum repetition time could be reduced further, the theoretical sensitivity increase in moving to an even shorter T_R is small. Therefore, scans were collected with a T_R of 20 ms as a typical value that could be used for multi-slice measurements in vivo.

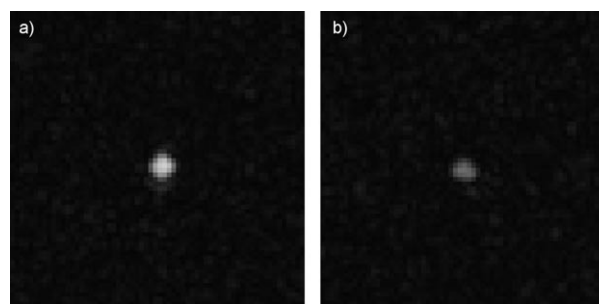


Figure 11. Gradient echo ^{19}F images of a) $[\text{Ho}(\text{L}^3)]$ and b) $[\text{Y}(\text{L}^3)]$ samples (4 mm). Samples were imaged by using an Ernst angle excitation of a 2 mm thick slice, in-plane resolution of $0.5 \times 0.7 \text{ mm}$, $T_E=1.56 \text{ ms}$, $T_R=20 \text{ ms}$ and 768 transients.

It is likely that the full theoretical enhancement was not observed in these imaging experiments due to several factors. At low T_R/T_1 ratios, a steady-state transverse magnetisation can be established which contributes constructively to image intensity particularly for $[\text{Y}(\text{L}^3)]$, hence yielding a greater SNR than expected. Loss of differential sensitivity is expected for $[\text{Ho}(\text{L}^3)]$ due to greater R_2 decay during the echo. Phase evolution of the signal arising from the second most abundant isomer of $[\text{Ho}(\text{L}^3)]$ during the echo time (2210 Hz offset) led to partial destructive cancellation of the imaging signal, reducing the observed signal to 0.83 of the expected strength that could be recovered through optimisation of T_E for in-phase imaging of both isomers. The experimental measured sensitivity enhancement is then more reliably estimated as 2.9. Finally, the theoretical enhancement is calculated based on uniform Ernst angle excitation across the entire sample; the small surface coil used for these studies provided high basic imaging sensitivity but a non-uniform flip angle that may differentially affect sensitivity.

Conclusions

The creation of paramagnetic fluorinated probes based on kinetically robust macrocyclic complexes of lanthanide(III) ions allows increases in sensitivity to be gained in both MRS and MRI experiments. Placing one (or more) trifluoromethyl groups between 5 and 7 Å from the paramagnetic centre in a complex gives rise to one major fluorine resonance signal associated with formation of a preferred isomer in solution. This means that longitudinal relaxation rate enhancements (versus diamagnetic analogues) of the order of 30 to 300 can be gained over a field range of 3 to 9.4 T by using Tm, Er, Ho and Tb complexes. This allows faster acquisition of data in a given time period and leads to an order of magnitude enhancement in signal intensity, for spectroscopy at least.

The first detailed analysis of the interplay between the applied field, the selection of Ln^{III} ion and the rotational correlation time allows predictions to be made about the design and selection of such probes. For the cases examined herein, complexes of Ho, Tb and Dy are likely to give rise to large increases in R_1 at lower field (<4.7 T) without incurring too great a loss in sensitivity through concomitant increases in R_2 and the observed linewidth. At fields of 7 T and above, complexes of Tm and Er may be more useful, to avoid the steeper increase in R_2 associated with the quadratic dependence on μ_{eff} (Curie broadening).

By permuting the lanthanide ion, ¹H/¹⁹F dual imaging studies may be undertaken by using complexes of Gd^{III} for the proton MRI work. Each complex will possess identical biodistributions in vivo, allowing the possibility of measuring local probe concentration in ¹⁹F studies. This may be particularly useful with responsive ¹H MRI probes, in which modulation of the relaxivity of the Gd^{III} complex is a function of both probe concentration and a given parameter, such as pH, pM or pX.

An advantage of ¹⁹F magnetic resonance studies is the exquisite sensitivity of the ¹⁹F shift of the reporter group to its local chemical environment. This sensitivity is enhanced in the paramagnetic complexes reported herein. By careful consideration of the location of the CF₃ reporter group, that is, its polar coordinates, it is possible to devise systems in which the shift non-equivalence of conformers of the same complex is over $\delta = 50$ ppm. A chemical transformation may alter the relative population of such isomers and allow the change to be monitored by studying the variation in the ratio of the two isomers. The differing behaviour of the *ortho*-substituted ester/carboxylate and *ortho*-cyano complexes [Ln(L^{6a}/L^{6b})] and [Ln(L^{4b})] affords a proof of principle.

In addition, responsive systems that give rise to a modulation of chemical shift of over $\delta = 20$ ppm have been defined to, for example, signal pH variation. The behaviour of the *ortho*-cyano complexes based on L^{4b} is most attractive in this respect because the difference in the ¹⁹F chemical shift observed between the two major isomers is a very sensitive function of pH, varying by $\delta = 14$ ppm for [Ho(L^{4b})] with a

pK_a of 7.1. Such behaviour augurs well for future chemical-shift imaging studies in which the observed parameter is independent of probe concentration. Finally, and by analogy with Gd contrast agent research, several paramagnetic fluorinated complexes could be conjugated to a biocompatible vector, the nature of which determines conjugate biodistribution and clearance rate. Examples based on L^{3b} are indicative.

Each of these aspects suggest a promising future for ¹⁹F magnetic resonance studies with such paramagnetic complexes, by using the switchable ¹H/¹⁹F probes that can be procured for current magnetic resonance instrumentation.

Experimental Section

Details of instrumentation, experimental procedures, analytical data and NMR spectral analyses are given in the Supporting Information.

DFT calculations: The DFT calculations were performed by using the Gaussian 03^[55] package for La³⁺ and Y³⁺ complexes; the structures of complexes of other lanthanides, including those of Y³⁺, are likely to be nearly identical. Importantly, however, the use of diamagnetic La³⁺ and Y³⁺ for DFT calculations avoids a host of largely unresolved theoretical issues with spin-orbit coupling and zero-field splitting in open-shell lanthanides. The Y³⁺ results were found to be very similar to those obtained with La³⁺, and given the similarity (± 0.02 Å) of the ionic radii of Ho³⁺, Y³⁺ and Er³⁺, only Y³⁺ complex computations are described herein. Gaussian 03^[55] logs and checkpoints are available from IK upon request.

Molecular geometries were optimised in vacuo by using spin-restricted B3LYP exchange-correlation functional with a compound basis set (cc-pVDZ for CHNOFS, Stuttgart ECP28MWB for Ln and WGBS for Y). Saddle points were located by using QST2 and QST3 methods. Hessians were computed and intrinsic reaction coordinates traced in both directions to ensure that the located saddle points were first-order saddles corresponding to the process under consideration.

¹⁹F NMR spectroscopic relaxation analysis: ¹⁹F NMR spectroscopic longitudinal relaxation times were measured in dilute solutions in D₂O (typically 1 mM) at 295 K by using the inversion-recovery technique, without proton decoupling, by using Varian spectrometers operating at magnetic inductions corresponding to fluorine frequencies of 188, 376, 470 and 658 MHz (Mercury-200, Mercury-400, Inova-500, VNMR-700), with chemical shifts reported relative to fluorotrichloromethane. The resulting free induction decays were subjected to backward linear prediction, optimal exponential weighting, zero filling, Fourier transform, phasing and baseline correction (by polynomial fitting to signal-free spectrum areas). The signals were integrated by using Lorentzian line fitting. Inversion-recovery type function was fitted to the resulting data by using Levenberg-Marquardt minimisation of the non-linear least squares error functional.

Proton relaxometric studies: The water proton $1/T_1$ longitudinal relaxation rates (20 MHz, 25 °C) were measured by using a Stellar Spinmaster Spectrometer (Mede, Pv, Italy) with aqueous solutions of the complexes (0.5–2 mM). The choice of this lower field allows better comparison with earlier literature data. For the T_1 determinations, the standard inversion-recovery method was used with a typical 90° pulse width of 3.5 μ s, 16 experiments of 4 scans. The reproducibility of the T_1 data was estimated to be $\pm 1\%$. The temperature was controlled by using a Stellar VTC-91 air-flow heater equipped with a copper-constantan thermocouple (uncertainty of 0.1 ± 0.1 °C). The proton $1/T_1$ NMRD profiles were measured by using a fast field-cycling Stellar Spinmaster FFC relaxometer over a continuum of magnetic field strengths from 0.00024 to 0.5 T (corresponding to 0.01–20 MHz proton Larmor frequencies). The relaxometer operates under computer control with an absolute uncertainty in $1/T_1$ of $\pm 1\%$. Data points from 0.47 (20 MHz) to 1.7 T (70 MHz) were collected by using a Stellar Spinmaster spectrometer operating at variable fields.

¹⁷O NMR spectroscopy: Variable-temperature ¹⁷O NMR spectra were recorded by using a JEOL ECP-400 (9.4 T) spectrometer equipped with a 5 mm probe and a standard temperature control unit. Aqueous solutions of the complexes (≈20–30 mM) containing 2.8% of the ¹⁷O isotope (Cambridge Isotope) were used. The observed transverse relaxation rates (R_2^{obs}) were calculated from the signal width at half height ($\Delta\nu_{1/2}$): $R_2^{\text{obs}} = \pi \times \Delta\nu_{1/2}$.

¹⁹F MRI: Fluorine-19 imaging data were collected by using a 7 T Varian Unity Inova micro-imaging system (Varian Inc., Palo Alto, California, USA) equipped with broadband capability, actively shielded gradients (180 μs rise time to 400 mT/m) and a purpose-built two-turn circular ¹⁹F surface coil (i.d. 12 mm, 281 MHz ¹⁹F frequency), which was used for both excitation and reception of the signal. Aqueous samples of the [Y(L³)] and [Er(L³)] complexes (200 μL, 4 mM) were prepared, placed in 5 mm NMR tubes and positioned on the axis of the coil. Conventional proton MRI was used to localise and shim the samples based on the proton water signal. Following ¹⁹F pulse calibration, R_1 values were determined for each sample by using a saturation recovery sequence (35 μs pulse, 22 experiments, 128 scans) to calculate Ernst angle pulses for optimal imaging sensitivity. Fluorine MR images were then collected by using a RF spoiled, gradient echo imaging sequence with a repetition time (T_R) of 20 ms, an echo time (T_E) 1.56 ms, a 0.5 ms sinc pulse for selection of a 6 mm thick slice, a 48 × 48 mm field of view, a 32 × 32 matrix and a 50 kHz receiver bandwidth. Relative imaging sensitivity for the two complexes was determined by region-of-interest analysis of the signal-to-noise ratio in each image.

Preparation of L² and its lanthanide(III) complexes

[4,7-Bis(tert-butoxycarbonylmethyl)-10-[(2-trifluoromethylphenylcarbamoyl)methyl]-1,4,7,10-tetraazacyclododec-1-yl]acetic acid tert-butyl ester: 2-Chloro-*N*-(2-trifluoromethylphenyl)acetamide (0.167 g, 0.91 mmol) was added to a stirred solution of 1,4,7-tris(tert-butoxycarbonylmethyl)-1,4,7,10-tetraazacyclododecane (0.30 g, 0.58 mmol), KI (≈10 mg, as catalyst) and K₂CO₃ (0.80 g, 0.58 mmol) in anhydrous CH₃CN (20 mL) at 85 °C under argon. The mixture was left to boil under reflux for 15 h, and gave a pale orange solution and a white precipitate. The precipitate was removed by filtration and the residue washed with CH₂Cl₂ (2 × 30 mL). The solvent was removed under reduced pressure and the resulting oil was purified by silica gel column chromatography (eluent: gradient, 100% CH₂Cl₂ → 5% CH₃OH/CH₂Cl₂) to give a pale brown oil (0.25 g, 61%). ¹H NMR (200 MHz, CDCl₃): δ = 1.43, (27H; CH₃), 2.02–3.66 (very br, 24H; CH₂ ring and CH₂CO), 7.28 (d, J = 8.0 Hz, 1H; ArH), 7.43 (d, J = 8.0, 1H; ArH), 7.56 (m, 2H; ArH), 9.97 ppm (s, 1H; NHCO); ¹³C NMR (125 MHz, CDCl₃): δ = 28.11 (CH₃), 49.04 (CH₂ ring), 53.68 (CH₂ ring), 55.89 (CH₂CO), 56.72 (CH₂CO), 82.13 (CCH₃), 123.84 (q, 1J (C,F) = 274 Hz, CF₃), 126.13 (q, 2J (C,F) = 30 Hz, CCF₃), 126.42 (3J (C,F) = 5 Hz, Ar), 129.40 (Ar), 132.35 (Ar), 134.50 (Ar), 135.58 (Ar), 172.29 (CO), 172.73 (CO), 173.16 ppm (CO); ¹⁹F NMR (200 MHz, CDCl₃): δ = –60.80 ppm (CF₃); MS (ESI): m/z : 716.3 [M+H]⁺; HRMS (ESI): m/z calcd for C₃₅H₅₆O₇N₃F₃Na: 738.4024; found: 738.4026.

[4,7-Bis(carboxymethyl)-10-[(2-trifluoromethylphenylcarbamoyl)methyl]-1,4,7,10-tetraazacyclododec-1-yl]acetic acid: Trifluoroacetic acid (3 mL) was added to a solution of [4,7-bis(tert-butoxycarbonylmethyl)-10-[(2-trifluoromethylphenylcarbamoyl)methyl]-1,4,7,10-tetraazacyclododec-1-yl]-acetic acid tert-butyl ester (0.23 g, 0.32 mmol) in CH₂Cl₂ (5 mL). The solution was stirred at RT for 2 h. The solvent was removed under reduced pressure and the resulting solid repeatedly washed with CH₂Cl₂ (5 × 5 mL) to give the product as a trifluoroacetate salt. The residue was dissolved in H₂O (5 mL) and left to stir for 2 h with anion exchange resin (DOWEX 1 × 8 200–400 Mesh, pre-treated with 1 M HCl) in water to give the chloride salt. The resin was removed by filtration and the solvent removed under reduced pressure to give a light yellow oil (0.13 g, 74%). ¹H NMR (400 MHz, CDCl₃): δ = 3.09–3.92 (very br, 16H; CH₂ ring), 7.25–7.94 ppm (brm, 4H; ArH); ¹⁹F NMR (200 MHz, CDCl₃): δ = –62.31 ppm (CF₃); MS (ES⁺) m/z : 570.4 [M+Na]⁺.

[Gd(L²): [4,7-Bis(carboxymethyl)-10-[(2-trifluoromethylphenylcarbamoyl)methyl]-1,4,7,10-tetraazacyclododec-1-yl]acetic acid (0.07 g, 0.13 mmol) was dissolved in H₂O (3 mL) and the pH adjusted to ≈6. [Gd(OAc)₃] (0.05 g, 0.14 mmol) was added to the solution, which was

subsequently left to boil under reflux for 3 h. Once cooled, the solvent was removed under reduced pressure and the complex purified by alumina chromatography (eluent: gradient, (5% MeOH/CH₂Cl₂ → 20% MeOH/CH₂Cl₂) (0.07 g, 77%). ¹⁹F NMR (376 MHz, D₂O): δ = –62.8 ppm (CF₃); MS (ESI): m/z : 701.3 [M–H][–], 725.2 [M+Na]⁺, 741.2 [M+K]⁺; HRMS (ESI): m/z calcd for C₂₃H₂₈O₇N₃F₃¹⁵⁵Gd: 698.1172; found: 698.1169.

The following complexes were prepared as described for [L²Gd]:

[Ho(L²): ¹H NMR (200 MHz, D₂O, pD = 5.5) partial: δ = –93.5, –79.3, –69.1, –58.23, –47.4, –36.0, –32.1, –12.4, –1.3, –1.1, 4.6, 7.6, 11.0, 12.9, 13.9, 14.9, 18.7, 23.0, 28.9, 44.2, 55.3, 86.3, 92.5 ppm; ¹⁹F NMR (376 MHz, D₂O): δ = –64.2 (CF₃, major species), –62.7, –62.1, –60.5, –57.9, –56.2, –54.2, –50.8 ppm (CF₃, minor species); MS (ESI): m/z : 732.1 [M+Na]⁺, 708.2 [M–H][–]; HRMS (ESI): m/z calcd for C₂₃H₂₈O₇N₃F₃¹⁶⁵Ho: 708.1250; found: 708.1250.

[Tm(L²): ¹H NMR (500 MHz, D₂O, pD = 5.5) partial: δ = –246.3, –215.5, –208.7, –150.7, –142.6, –119.6, –111.4, –92.6, –80.5, –71.9, –25.3, –18.3, 18.9, 24.6, 35.9, 37.6, 40.0, 45.7, 49.3, 64.4, 79.3, 320.6, 325.7, 340.2, 380.0 ppm; ¹⁹F NMR (188 MHz, D₂O): δ = –75.9 (CF₃, major species), –88.1, –87.3, –80.77, –77.4, –66.8, –49.5 ppm (CF₃, minor species); MS (ESI): m/z : 736.2 [M+Na]⁺, 712.2 [M–H][–]; HRMS (ESI): m/z calcd for C₂₃H₂₈O₇N₃F₃¹⁶⁹Tm: 712.1289; found: 708.1286.

[Er(L²): ¹H NMR (500 MHz, D₂O, pD = 5.5) partial: δ = –101.7, –89.9, –84.4, –80.4, –71.4, –66.5, –57.6, –56.0, –38.1, –32.1, –29.5, –8.0, –2.9, 12.8, 14.6, 15.9, 18.7, 21.9, 33.4, 128.9, 136.4, 145.0, 153.9, 164.0 ppm; ¹⁹F NMR (188 MHz, D₂O): δ = –64.8 (CF₃, major species), –76.2, –70.4, –69.2, –62.7, –61.8, –58.3, –54.8 ppm (CF₃, minor species); MS (ESI): m/z : 709.3 [M–H][–], 751.2 [M+K]⁺; HRMS (ESI): m/z calcd for C₂₃H₂₈O₇N₃F₃¹⁶⁶Er: 709.1249; found: 709.1240.

[Tb(L²): ¹⁹F NMR (188 MHz, D₂O): δ = –51.9 (CF₃, major species), –60.2, –44.9, –39.8, –36.7 ppm (CF₃, minor species); MS (ESI): m/z : 742.1 [M+Na]⁺, 702.2 [M–H][–]; HRMS (ESI): m/z calcd for C₂₃H₂₈O₇N₃F₃¹⁵⁹Tb: 702.1198; found: 702.1189; τ(H₂O) 1.76 ms, ττ(D₂O) 2.78 ms; q_{Tb} = 0.75 (±0.1).

[Y(L²): ¹⁹F NMR (188 MHz, D₂O): δ = –62.0 ppm; MS (ESI): m/z : 656.2 [M+Na]⁺, 632.2 [M–H][–]; HRMS (ESI): m/z calcd for C₂₃H₂₈F₃N₃O₇Na⁸⁹Y: 656.0969; found: 656.0970.

Acknowledgements

We thank ESF COST Action D38 and the EC networks of excellence EMIL and DiMI for support. This work was supported by the EPSRC (EP/F065205/1, EP/H003789/1) and the NSCCS.

- [1] P. L. Choyke, A. J. Dwyer, M. V. Knopp, *J. Magn. Reson. Imaging* **2003**, *17*, 509; A. R. Padhani, J. E. Husband, *Clin. Radiol.* **2001**, *56*, 607; M. V. Knopp, F. L. Giesel, H. Marcos, H. von-Tengg-Kobligk, P. L. Choyke, *Top. Magn. Reson. Imaging* **2001**, *12*, 301.
- [2] J. A. Bergwerff, A. A. Lysova, L. Espinosa-Alonso, I. V. Koptuyg, B. M. Weckhuysen, *Chem. Eur. J.* **2009**, *15*, 2363; I. V. Koptuyg, A. V. Khomichev, A. A. Lysova, R. Z. Sagdeev, *J. Am. Chem. Soc.* **2008**, *130*, 10452.
- [3] S. J. Karlik, R. Bartha, K. Kennedy, R. Chhem, *AJR* **2007**, *189*, 105; F. J. Ruhli, H. von Waldburg, S. Nielles-Vallespin, T. Boni, P. Speier, *JAMA* **2007**, *298*, 2618.
- [4] C. Corot, P. Robert, J.-M. Idee, M. Port, *Adv. Drug Delivery Rev.* **2006**, *58*, 1471; A. K. Gupta, M. Gupta, *Biomaterials* **2005**, *26*, 3995; H.-J. Weinmann, W. Ebert, B. Misselwitz, H. Schmitt-Willich, *Eur. J. Radiol.* **2003**, *46*, 33.
- [5] A. E. Merbach, E. Toth, E. eds. 'The Chemistry of Contrast Agents in Medical Magnetic Resonance Imaging', Wiley, New York, **2001**; P. Caravan, J. J. Ellison, T. J. McMurry, R. B. Lauffer, *Chem. Rev.* **1999**, *99*, 2293; P. Caravan, *Chem. Soc. Rev.* **2006**, *35*, 512; P. S. Tofts, J.

- Magn. Reson. Imaging* **1997**, *7*, 91; S. Aime, M. Botta, E. Terreno, *Adv. Drug Delivery Rev.* **2005**, *57*, 173.
- [6] A. R. Padhani, *J. Magn. Reson. Imaging* **2002**, *16*, 407; A. R. Padhani, J. E. Husband, *Clin. Radiol.* **2001**, *56*, 607.
- [7] M. Higuchi, Y. Matsuba, K. Sato, T. C. Saïdo, *Nat. Neurosci.* **2005**, *8*, 527; W. G. Schreiber, B. Eberle, S. Laukemper-Ostendorf, K. Markstaller, N. Weiler, A. Scholz, K. Burger, C. P. Heussel, M. Thelen, H. U. Kauczor, *Magn. Reson. Med.* **2001**, *45*, 605; R. C. Samaratunga, R. G. Pratt, Y. Zhu, R. J. Massoth, S. R. Thomas, *Med. Phys.* **1999**, *21*, 697; V. D. Mehta, P. V. Kulkarni, R. P. Mason, A. Constantinescu, S. Aravind, N. Gamer, P. P. Antich, *FEBS Lett.* **1994**, *349*, 234; C. J. Deutsch, J. S. Taylor, *Biophys. J.* **1989**, *55*, 799.
- [8] a) M. Xia, V. D. Kodibagkar, H. Liu, R. P. Mason, *Phys. Med. Biol.* **2006**, *51*, 45; b) R. Weissleder, M. J. Pittet, *Nature* **2008**, *452*, 580; c) J. M. Janjic, M. Srinivas, D. K. K. Kadayakkara, D. T. Ahrens, *J. Am. Chem. Soc.* **2008**, *130*, 2832; d) J. W. Bulte, *Nat. Biotechnol.* **2005**, *23*, 945.
- [9] a) E. T. Ahrens, R. Flores, H. Y. Xu, P. A. Morel, *Nat. Biotechnol.* **2005**, *23*, 983; b) Y. Yu, V. D. Kodibagkar, W. Cui, R. P. Mason, *Curr. Med. Chem.* **2005**, *12*, 819; c) J. Maki, C. Masuda, S. Morikawa, M. Morita, T. Innbushi, Y. Matsusue, H. Taguchi, I. Tooyamin, *Biomaterials* **2007**, *28*, 434; d) J. C. Jackson, J. T. Hammill, R. A. Mehl, *J. Am. Chem. Soc.* **2007**, *129*, 1160; e) H. R. Kalbitzer, G. Rohr, E. Nowak, R. S. Goody, W. Kuhn, H. Zimmerman, *NMR Biomed.* **1992**, *5*, 347; f) J. W. Peng, *J. Magn. Reson.* **2001**, *153*, 32; g) H. Khan, I. Kuprov, T. D. Craggs, P. J. Hore, S. E. Jackson, *J. Am. Chem. Soc.* **2006**, *128*, 10729.
- [10] a) L. D. Stegman, A. Rehemtulla, B. Beattie, A. Kievit, T. S. Lawrence, R. G. Blasberg, J. G. Tjuvajev, B. D. Ross, *Proc. Natl. Acad. Sci. USA* **1999**, *96*, 9821; b) W. E. Hull, R. E. Port, R. Herrmann, B. Britsch, W. Kunz, *Cancer Res.* **1988**, *48*, 1680; c) W. Wolf, M. J. Al-bright, M. S. Silver, H. Weber, U. Reichardt, R. Sauer, *Magn. Reson. Imaging* **1987**, *5*, 165.
- [11] a) N. J. Baldwin, Y. Wang, T. C. Ng, *Magn. Reson. Imaging* **1996**, *14*, 275; b) W. Du, A. M. Nyström, L. Zhang, K. T. Powell, Y. Li, C. Cheng, S. A. Wickline, K. C. Wooley, *Biomacromolecules* **2008**, *9*, 2826; c) C. Fogel, Z. Ding, H. Harding, S. Jander, G. Reichmann, C. Jacoby, R. Schubert, J. Schrader, *J. Circulation* **2008**, *118*, 140; d) K. C. Partlow, J. Chen, J. A. Brant, A. M. Neubauer, T. E. Meyerrose, M. H. Creer, J. A. Nolte, S. D. Caruthers, G. M. Lanza, S. A. Wickline, *FASEB J.* **2007**, *21*, 1647.
- [12] a) V. D. Kodibagkar, J. Yu, L. Liu, H. P. Hetherington, R. P. Mason, *Magn. Reson. Imaging* **2006**, *24*, 959; b) S. Mizukami, R. Takikawa, F. Sugihara, Y. Heri, H. Tochio, M. Waelchli, M. Shirakawa, K. Kikuchi, *J. Am. Chem. Soc.* **2008**, *130*, 794; c) M. Oishi, S. Sumitani, Y. Nagasaki, *Bioconjugate Chem.* **2007**, *18*, 1379; d) K. Tanaka, N. Kitamura, K. Naka, Y. Chujo, *Chem. Commun.* **2008**, 6176; e) J. X. Yu, P. Otten, Z. Y. Ma, W. N. Cui, L. Liu, R. P. Mason, *Bioconjugate Chem.* **2004**, *15*, 1334.
- [13] a) P. K. Senanayake, A. M. Kenwright, D. Parker, S. van der Hoorn, *Chem. Commun.* **2007**, 2923; b) A. M. Kenwright, I. Kuprov, E. De Luca, D. Parker, S. U. Pandya, P. K. Senanayake, D. G. Smith, *Chem. Commun.* **2008**, 2514.
- [14] D. Parker, P. K. Senanayake, Int. Pat. Appl. WO2008/132433 (PCT/GB 2008 1001284).
- [15] R. H. Carr, J. Hernalsteen, *J. Appl. Polym. Sci.* **1994**, *52*, 1015.
- [16] H. Lee, R. R. Price, G. E. Holburn, C. L. Partain, M. D. Adams, W. P. Cacheris, *J. Magn. Reson. Imaging* **1994**, *4*, 609.
- [17] a) S. Aime, A. Barge, M. Botta, D. Parker, A. S. de Sousa, *J. Am. Chem. Soc.* **1997**, *119*, 4767; b) S. Aime, A. Barge, J. I. Bruce, M. Botta, J. A. K. Howard, J. M. Moloney, D. Parker, A. S. de Sousa, M. Woods, *J. Am. Chem. Soc.* **1999**, *121*, 5762.
- [18] E. Terreno, M. Botta, P. Boniforte, C. Bracco, L. Milone, B. Mandino, F. Uggeri, S. Aime, *Chem. Eur. J.* **2005**, *11*, 5531.
- [19] a) B. Bleaney, *J. Magn. Reson.* **1972**, *8*, 91; b) I. Bertini, C. Luchinat, G. Parigi, *Progr. Nucl. Magn. Reson. Spectrosc.* **2002**, *40*, 249; c) I. Bertini, I. Capozzi, C. Luchinat, G. Nicastro, Z. C. Xia, *J. Phys. Chem.* **1993**, *97*, 6351.
- [20] a) A. Harrison, C. A. Walker, K. Pereira, L. Royle, D. Parker, K. Pulukkody, T. J. Norman, *Magn. Reson. Imaging* **1993**, *11*, 761; b) K. Pulukkody, T. J. Norman, D. Parker, L. Royle, C. J. Broan, *J. Chem. Soc. Perkin Trans. 2* **1993**, 605; c) D. Parker, *Chem. Soc. Rev.* **1990**, *19*, 271; d) C. J. Broan, J. P. L. Cox, A. S. Craig, R. Katakya, A. Harrison, D. Parker, A. M. Randall, G. Ferguson, *J. Chem. Soc. Perkin Trans. 2* **1991**, 87; e) A. Harrison, C. Walker, J. P. L. Cox, K. J. Jan-kowski, J. Sansom, M. A. W. Eaton, N. R. A. Beeley, A. T. Millican, D. Parker, *Int. J. Nucl. Med. Biol.* **1991**, *18*, 469.
- [21] a) P. Wedeking, K. Kumar, M. F. Tweedle, *Magn. Reson. Imaging* **1992**, *10*, 641; b) M. F. Tweedle, P. Wedeking, K. Kumar, *Invest. Radiol.* **1995**, *30*, 372.
- [22] L. Helm, *Progr. NMR Spec.* **2006**, *49*, 45–64.
- [23] R. Sharp, L. Lohr, J. Miller, *Progr. NMR Spec.* **2001**, *38*, 115–158.
- [24] J. Kowalewski, L. Nordski, N. Benetis, P.-O. Westlund, *Progr. NMR Spec.* **1985**, *17*, 141–185.
- [25] M. Gueron, *J. Magn. Reson.* **1975**, *19*, 58–66.
- [26] J. Kowalewski, C. Luchinat, T. Nilsson, G. Parigi, *J. Phys. Chem. A* **2002**, *106*, 7376–7382.
- [27] J. H. Freed, *J. Chem. Phys.* **1968**, *49*, 376–&.
- [28] R. Kubo, *Hyperfine Interact.* **1981**, *8*, 731–738.
- [29] A. G. Redfield, *IBM J. Res. Dev.* **1957**, *1*, 19–31.
- [30] R. K. Wangsness, F. Bloch, *Phys. Rev.* **1953**, *89*, 728–739.
- [31] M. Goldman, *J. Magn. Reson.* **2001**, *149*, 160–187.
- [32] E. Meirovitch, Y. E. Shapiro, A. Polimeno, J. H. Freed, *J. Phys. Chem. B* **2007**, *111*, 12865–12875.
- [33] E. Meirovitch, Y. E. Shapiro, A. Polimeno, J. H. Freed, *J. Phys. Chem. A* **2006**, *110*, 8366–8396.
- [34] E. Meirovitch, Y. E. Shapiro, Z. C. Liang, J. H. Freed, *J. Phys. Chem. B* **2003**, *107*, 9898–9904.
- [35] A. Abragam, *The principles of nuclear magnetism*; Clarendon Press: Oxford, **1961**.
- [36] M. Goldman, *J. Magn. Reson.* **1984**, *60*, 437–452.
- [37] N. Bloembergen, *The Journal of Chemical Physics* **1957**, *27*, 572–573.
- [38] J. A. Peters, J. Huskens, D. J. Raber, *Progr. NMR Spec.* **1996**, *28*, 283–350.
- [39] I. Kuprov, T. D. Craggs, S. E. Jackson, P. J. Hore, *J. Am. Chem. Soc.* **2007**, *129*, 9004–9013.
- [40] I. Kuprov, N. Wagner-Rundell, P. J. Hore, *J. Magn. Reson.* **2007**, *184*, 196–206.
- [41] S. L. Grage, U. H. N. Durr, S. Afonin, P. K. Mikhailiuk, I. V. Komarov, A. S. Ulrich, *J. Magn. Reson.* **2008**, *191*, 16–23.
- [42] C. S. Yannoni, B. P. Dailey, G. P. Ceasar, *J. Chem. Phys.* **1971**, *54*, 4020.
- [43] a) S. Amin, D. A. Voss, W. D. Horrocks, C. H. Lake, M. R. Churchill, J. R. Morrow, *Inorg. Chem.* **1995**, *34*, 3294; b) S. Aime, A. Barge, M. Botta, D. Parker, A. S. de Sousa, *J. Am. Chem. Soc.* **1997**, *119*, 4767.
- [44] R. S. Dickens, J. A. K. Howard, J. M. Moloney, D. Parker, R. D. Peacock, *Angew. Chem.* **1997**, *109*, 541; *Angew. Chem. Int. Ed. Engl.* **1997**, *36*, 521.
- [45] a) R. S. Dickens, J. A. K. Howard, C. L. Maupin, J. M. Moloney, D. Parker, J. P. Riehl, G. Siligardi, J. A. G. Williams, *Chem. Eur. J.* **1999**, *5*, 1095; b) S. Aime, A. Barge, M. Botta, J. A. K. Howard, J. M. Moloney, D. Parker, A. S. de Sousa, M. Woods, *J. Am. Chem. Soc.* **1999**, *121*, 5762.
- [46] a) S. Aime, P. L. Anelli, M. Botta, F. Fedeli, M. Grandi, P. Paoli, F. Uggeri, *Inorg. Chem.* **1992**, *31*, 2422; b) S. Aime, M. Botta, D. Parker, J. A. G. Williams, *J. Chem. Soc. Dalton Trans.* **1995**, 2259.
- [47] R. D. Shannon, *Acta Crystallog. Sect. A: Cryst. Phys. Diffr. Theor. Gen. Crystallogr.* **1976**, *32*, 751.
- [48] H. Lammers, F. Maton, D. Pubanz, M. W. Van Laren, H. Van Bekkum, A. E. Merbach, R. N. Muller, J. A. Peters, *Inorg. Chem.* **1997**, *36*, 2527.
- [49] A. L. Thompson, D. Parker, D. A. Fulton, J. A. K. Howard, S. U. Pandya, H. Puschmann, K. Senanayake, P. A. Stenson, A. Badari, M. Botta, S. Avedano, S. Aime, *Dalton Trans.* **2006**, 5606.
- [50] D. Parker, *Chem. Soc. Rev.* **2004**, *33*, 156; S. Aime, M. Botta, D. Parker, J. A. G. Williams, *J. Chem. Soc. Dalton Trans.* **1995**, 2259; S.

- Aime, M. Botta, D. Parker, J. A. G. Williams, *J. Chem. Soc. Dalton Trans.* **1996**, 17.
- [51] S. Aime, A. S. Batsanov, M. Botta, J. A. K. Howard, D. Parker, K. Senanayake, J. A. G. Williams, *Inorg. Chem.* **1994**, 33, 4696.
- [52] T. J. Swift, R. J. Connick, *J. Chem. Phys.* **1962**, 37, 307.
- [53] A. Beeby, I. M. Clarkson, R. S. Dickins, S. Faulkner, D. Parker, L. Royle, A. S. de Sousa, J. A. G. Williams, M. Woods, *J. Chem. Soc. Perkin Trans. 2* **1999**, 493.
- [54] R. R. Ernst, W. A. Anderson, *Rev. Sci. Instrum.* **1966**, 37, 93.
- [55] Gaussian 03, Revision E.01, M. J. Frisch, G. W. Trucks, H. B. Schlegel, G. E. Scuseria, M. A. Robb, J. R. Cheeseman, J. A. Montgomery, Jr., T. Vreven, K. N. Kudin, J. C. Burant, J. M. Millam, S. S. Iyengar, J. Tomasi, V. Barone, B. Mennucci, M. Cossi, G. Scalmani, N. Rega, G. A. Petersson, H. Nakatsuji, M. Hada, M. Ehara, K. Toyota, R. Fukuda, J. Hasegawa, M. Ishida, T. Nakajima, Y. Honda, O. Kitao, H. Nakai, M. Klene, X. Li, J. E. Knox, H. P. Hratchian, J. B. Cross, V. Bakken, C. Adamo, J. Jaramillo, R. Gomperts, R. E. Stratmann, O. Yazyev, A. J. Austin, R. Cammi, C. Pomelli, J. W. Ochterski, P. Y. Ayala, K. Morokuma, G. A. Voth, P. Salvador, J. J. Dannenberg, V. G. Zakrzewski, S. Dapprich, A. D. Daniels, M. C. Strain, O. Farkas, D. K. Malick, A. D. Rabuck, K. Raghavachari, J. B. Foresman, J. V. Ortiz, Q. Cui, A. G. Baboul, S. Clifford, J. Cioslowski, B. B. Stefanov, G. Liu, A. Liashenko, P. Piskorz, I. Komaromi, R. L. Martin, D. J. Fox, T. Keith, M. A. Al-Laham, C. Y. Peng, A. Nanayakkara, M. Challacombe, P. M. W. Gill, B. Johnson, W. Chen, M. W. Wong, C. Gonzalez, J. A. Pople, Gaussian, Inc., Wallingford CT, **2004**

Received: August 19, 2009
Published online: December 2, 2009